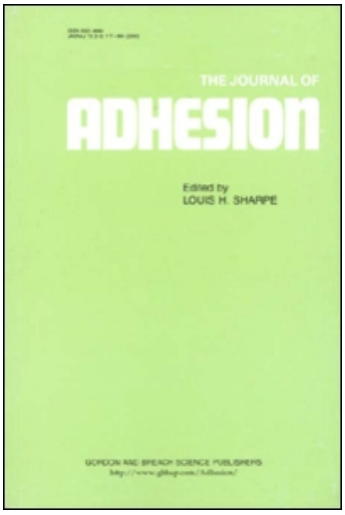

The Journal of Adhesion

Publication details, including instructions for authors and subscription information:
http://www.informaworld.com/smpp/title~content=t713453635

Cohesive Zone Models and Fracture

C. Y. Hui[a]; A. Ruina[a]; R. Long[a]; A. Jagota[b]
[a] Department of Mechanical and Aerospace Engineering, Cornell University, Ithaca, New York, USA [b] Department of Chemical Engineering and Bioengineering Program, Lehigh University, Bethlehem, Pennsylvania, USA

Online publication date: 20 January 2011

To cite this Article Hui, C. Y. , Ruina, A. , Long, R. and Jagota, A.(2011) 'Cohesive Zone Models and Fracture', The Journal of Adhesion, 87: 1, 1 — 52
To link to this Article: DOI: 10.1080/00218464.2011.538315
URL: http://dx.doi.org/10.1080/00218464.2011.538315

The Journal of Adhesion, 87:1–52, 2011

ISSN: 0021-8464 print/1545-5823 online
DOI: 10.1080/00218464.2011.538315

Taylor & Francis
Taylor & Francis Group

Cohesive Zone Models and Fracture

C. Y. Hui[1], A. Ruina[1], R. Long[1], and A. Jagota[2]
[1]Department of Mechanical and Aerospace Engineering, Cornell University, Ithaca, New York, USA
[2]Department of Chemical Engineering and Bioengineering Program, Lehigh University, Bethlehem, Pennsylvania, USA

Basic concepts on cohesive models and their usage in fracture are reviewed.

These included potential based cohesive zone models and the concept of an anisotropic failure surface. Some new results are presented for history-dependent cohesive zone models. In particular, a class of cohesive zone models where damage is represented by a state variable which evolves according to loading history is studied. The connection between cohesive zone model and crack nucleation is explored.

Keywords: Crack; Interface; Nucleation; Stress intensity factor

1. INTRODUCTION

There are at least two broad approaches to the mechanics of fracture. The first, initiated by Griffith, treats the crack-tip as infinitely sharp, with the result that stress and strain fields generally diverge at that point but a finite energy release rate can often be found. Crack equilibrium and stability can then be written by equating either the pre-factor on singular stress fields, the stress intensity factor, or the energy-release-rate, to material properties that describe resistance to fracture, *e.g.*, the fracture toughness. In the second approach, one introduces a traction-separation model, characteristic of the material

Received 16 March 2010; in final form 24 August 2010.

One of a Collection of papers honoring David A. Dillard, the recipient in February, 2010 of *The Adhesion Society Award for Excellence in Adhesion Science, Sponsored by 3 M.*

Address correspondence to C. Y. Hui, Department of Mechanical and Aerospace Engineering, Cornell University, 322 Thurston Hall, Ithaca, NY 14853, USA. E-mail: ch45@cornell.edu; chung-yuen.hui@gmail.com

and usually with finite tractions, at the crack-tip. As a consequence, stresses everywhere remain bounded and the sharp crack tip is replaced by a cohesive zone. In several cases, *e.g.*, linear-elastic materials where the cohesive zone is small compared with any other dimension, the two approaches provide asymptotically identical criteria for crack equilibrium and stability.

Since their introduction by Barenblatt in 1962 [1], cohesive zone models have been used to study a wide variety of physical phenomena, for example, crack growth along a prescribed plane in elastic-plastic and viscoelastic materials [2–7], adhesive contact of non-conforming surfaces [8–11], frictional sliding and earthquakes [12–14], sintering of polymeric particles [15], crazing in polymer glass [16–20], adhesion [21–23], fiber bridging and debonding in composite materials [24–29], fracture of adhesive joints [30], and stability of interfaces [19,31–34].

Before 1987, the usage of the cohesive zone model had been primarily restricted to the study of failure of preexisting cracks either in the opening or sliding mode, but not both. To study fracture in multiphase materials with complicated geometries, it is necessary to couple the shear and normal deformations in the cohesive model. Such an approach was used by Needleman to study the nucleation of voids from inclusions or second-phase particles in metals or composites [29]. This work spurred a large number of studies in the area of interface fracture and cohesive modeling in multiphase materials, see for example [35–44] and the references therein. In the past 10 years, cohesive zone models have been employed to study fragmentation [44–49] and crack initiation and growth in rate dependent materials [50]. One reason for their great popularity is that, in the computational setting, the cohesive zone model approach can be implemented in a very general manner, for example, allowing simulation of multiple interacting cracks that nucleate, grow, and heal spontaneously in a material as dictated by the history of its loading.

Works on cohesive zone models fall roughly into two categories. In the first, the cohesive zone model is used as a convenient theoretical substitute for, say, critical fracture toughness, to model material failure. For example, it can be used to study how cracks nucleate and grow in a structure. This relies on our ability to establish a relationship between interface fracture toughness and the cohesive parameters. With few exceptions, in such cases cohesive zone models are phenomenological in nature. In other words, there is no direct connection between the mathematical models and the underlying physical separation/sliding processes. Typically, a mathematical form of the cohesive zone model is assumed. For example, in Needleman's model [29,40], the cohesive traction is assumed to be the gradient of a work

potential. The parameters in these models may not bear any relation to the actual failure processes in the molecular or micro-structural scale. As alluded to earlier, in certain circumstances this last fact is of little consequence. For example, say we wish to model crack propagation in a linearly elastic material subjected to small strains in which the cohesive zone remains small compared with all relevant dimensions (small scale yielding). Then, all that matters is that the work of separation in the cohesive zone model be matched to the fracture toughness. That is, other details such as the maximum cohesive stress, characteristic cohesive zone opening, and the particular functional form relating these two quantities are not of consequence. However, if one introduces nearly any deviation from these ideal conditions, *e.g.*, inelasticity of material response, then the details of the cohesive zone model usually do matter significantly.

Cohesive parameters can sometimes be determined by fitting numerical simulations of fracture tests to experimental data. The hope is that extracted parameters represent material properties and can be used to model fracture of the same material under different loading conditions. However, this (usually implicit) assumption is often not satisfied and, as a consequence, the cohesive parameters are not unique; their values depend on specimen geometry and loading history. In this approach, the best possible outcome is that parameters determined based on different loading conditions or geometries are confined to small regions in the parameter space. This approach has been successfully applied to predicting interface fracture in a class of specimens. For example, Yang *et al.* [51,52] described how Mode I and Mode II cohesive zone parameters can be extracted from fracture testing of plastically deformed adhesive joints. Andena *et al.* [53] describe in some detail how cohesive zone parameters have been obtained for fracture in polybutene by using three different specimens (compact tension, single edge notched bending, and circumferentially notched tensile configurations). Zhou *et al.* [54] have similarly shown how cohesive zone parameters extracted from one test can be used to simulate another. Using cleavage of mica, Hill *et al.* [55] have shown how the cohesive stress and work of fracture can be determined independently from a single experiment. A brief review and discussion of cohesive zone models for polymer interfaces can be found in Rahul-Kumar *et al.* [43].

When interfacial deformations are restricted to a single mode, attempts have been made to deduce the mathematical form of the cohesive zone model from micromechanical modeling. An example of such an approach is the study of fiber bridging in fiber-reinforced composites [25,26]. These micromechanical-based models involve a

number of unknown material parameters, some of which can be inferred from material characterization tests. For example, the bridging law due to fiber pull-out may involve the interfacial shear strength of the fiber/matrix interface. This parameter can be determined by performing a single filament composite test. An exact analysis of this test can be found in [56]. A well-developed example of this approach is the modeling of crazes in glassy polymers. The crazed region can be treated as a cohesive zone. A large number of independent experiments have been carried out to measure characteristics of the microstructure of crazes, the traction on the craze-bulk interface, the opening displacements of the craze interface, the size and structure of the drawing zone, etc. For details, see [57,58] and references therein. These experimental approaches are supplemented by the development of physically based theory and molecular dynamics simulations to model the micromechanics of crazing, resulting in a close connection between cohesive and molecular parameters [59–61]. These simulations and theories have been checked against experiments with different geometries and material properties. For example, the polymer or the molecular weight of the polymer can be altered, or different molecular connectors on the interface between the polymer and the substrate can be used to study the effect on craze breakdown [62]. For air crazes, our current knowledge is sufficiently complete that one can create a cohesive zone model without adjustable parameters.

Therefore, in addition to the computational and modeling advantages cited earlier, a great strength of the cohesive zone approach is that it provides a link between physical models for crack-tip damage processes and the mechanics of the larger structure. Unfortunately, the painstaking work of representing and validating crack-tip physics with cohesive zone models has been carried out in only a few cases. Just as classical force field packages, such as those used in molecular dynamics simulations, capture a large range of interatomic and intermolecular interactions, one can envisage the development of an entire family of validated cohesive material models that could be collected into an analogous "force field."

A different approach is to uncover directly the constitutive description of surface decohesion/sliding by experiment. In general, these experiments are difficult to carry out since the stress and the deformation in the sample has to be spatially homogenous. Since cohesive zone models are often used to study crack nucleation and stability of interfaces, variation of the interfacial traction as interfacial slip or opening progresses, even if very small, is of primary importance. Failure of an interface is associated with decreasing traction as interfacial slip or opening progresses, *i.e.*, interfacial softening. Measuring the

response of the interface in the softening regime requires the design of very stiff loading devices. Examples of such approaches can be found in the rock friction literature, see for example [12, 13] and the references within.

The second category of cohesive modeling is concerned mostly with the development of computational schemes and numerical implementation and is not the focus of this work. References on these subjects can be found in [63].

In comparison with the large number of works in the two categories mentioned above, far less attention has been paid to understanding cohesive models from the point of view of constitutive modeling. For example, there have been very few discussions on the deficiencies and limitations of cohesive zone models currently used in the literature (a recent exception is the work by Jirasek and Zimmermann [42]). The concept of interfacial displacement or displacement discontinuity in the continuum description is often taken for granted. For example, it is often assumed that the interfacial displacements that enter into the constitutive model are identical to the experimental interfacial separations, whereas in reality these two quantities can differ significantly.

The plan of this paper is as follows: in Section 2 we attempt to give a clear definition of interfacial displacement. We also consider some widely used cohesive zone models and discuss their deficiencies. We also introduce the concept of a potential or yield surface in traction space. Here we attempt to draw an analogy between cohesive zone models and classical plasticity. Section 3 introduces the concept of a failure surface which may resolve some of the deficiencies highlighted in Section 2. In Section 4 we consider a state variable cohesive zone model with particular focus on rate independent models. Some consequences of these models in mixed mode fracture problems are discussed. Section 5 discusses the stability of cohesive zone interfaces and its connection to crack nucleation. We end with summary and discussion in Section 6.

2. CONSTITUTIVE RELATION OF COHESIVE ZONE MODEL

2.1. Continuum ''Point'' on an Interface

The existence of a constitutive relation requires the concept of a continuum "point". A continuum "point" is a region of the interface between the solids with a characteristic dimension, P, in the plane of the interface. It may include *a thin layer of the adjacent solids of characteristic size, H,* in a direction normal to the interface. The size of P and H must be negligible in comparison with all relevant

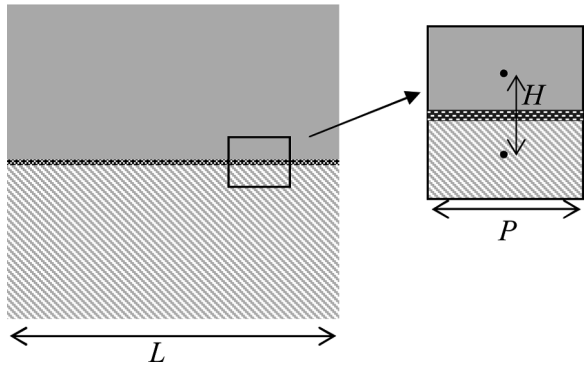

FIGURE 1 Schematic drawing of a continuum point. L is a characteristic length scale of the continuum problem (*e.g.*, specimen size, crack length, etc.). P and H denote the size scale of the continuum point. The continuum stress and strain fields are approximately homogeneous over the length scales P and H.

geometric dimensions, L, in the continuum problem. Figure 1 shows a region of a solid that includes a planar interface that may undergo opening or slip. The point is assumed to include many microscopic features (see Fig. 2 as an example). These microscopic features may include molecular chain scission or pull-out in polymers, asperities that deform and fracture in frictional sliding, micro-void formation,

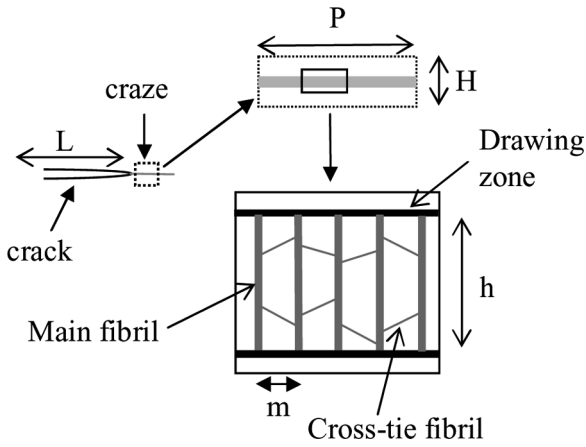

FIGURE 2 An example of the micro-structures inside a craze. P, H denote the size of the continuum point.

growth and coalescence in metals and elastomers, drawing and formation of craze fibrils in polymer glasses, slipping at the fiber/matrix interface, and breaking of fibers and fiber pull-out in fiber-reinforced composites. Smaller features can also be represented by the point, *e.g.*, intermolecular or interatomic interactions such as Van der Waals, hydrogen, and ionic bonding. In other words, these micro-nano-mechanical elements have a wide range of characteristic sizes and a continuum point may include many of these mechanisms. Let m be the characteristic size of these elements in the plane of the interface and h be their characteristic size normal to the interface. For example, $m, h \approx$ Å for interatomic interactions, $m \approx nm$ for craze fibrils and dislocations, $m \approx \mu m$ or higher for voids, $h \approx \mu m$ for crazes, and $h \approx mm$ for fiber pull-out. Thus, for the continuum description to be legitimate, a hierarchy of size scales is implicit, such that $L >> P >> m, h$. In addition, over a wide range of length scales, the constitutive relation must be independent of the size of the continuum point.

In Barenblatt's theory, separation of two surfaces is opposed by interatomic or intermolecular forces so that the traction across the cohesive zone is the gradient of an interatomic potential. In this case, $m, h \approx$ Å, and the value of fracture toughness approaches twice the surface energy. For most material systems this theory is too simplistic, since, even in nearly ideal-brittle materials such as glass and mica, the fracture toughness is much higher than twice the surface energy. This is because, for most materials, the interatomic forces required for separation are much higher than those required to initiate some form of damage (*e.g.*, cavitation, flow, or crazing). Therefore, the material invariably suffers some form of inelastic deformation near the crack tip, resulting in much greater energy dissipation. Even in the few cases where fracture toughness does indeed equal twice the surface energy, as in separation of carefully-prepared elastomers [64], the cohesive stress is much smaller than would be expected on the basis of intermolecular interactions between continuous bodies [65]. This fact is typical; the characteristic stress (displacement) to open an interface is much smaller (larger) than predicted on the basis of intermolecular forces.

Consider, for example, the fracture of rubber. Based on the typical number of chains ($\approx 10^{18}/m^2$) that cross a fracture plane and the energy needed to break a chemical bond ($\approx 400\ kJ/mole$), the surface energy should be about 1–2 J/m^2 [66]. Experimental values of fracture energies, however, range from 10 to 1000 J/m^2 [66]. The stress needed to completely separate an interface with energy of a few J/m^2 based on short-range intermolecular forces (acting over a few nm) has values on the order of GPa, which is at least three orders of magnitude higher

than the small strain elastic modulus ($E \approx 1\,MPa$) of a typical elastomer. Crack growth can occur by at least two mechanisms: in the first, the highly stretched polymer chains directly ahead of the crack tip break. As pointed out by Lake and Thomas [66], since all the bonds in a chain are stretched to their breaking point, when one of the bonds breaks, the entire chain relaxes to zero load and thus all of the stored elastic energy in the chain is lost. The energy dissipation per molecule is thus proportional to number of bonds, n, in a chain between cross-links. (Since the number of chains crossing an interface scales as the $n^{-1/2}$, the energy per unit area increases as $n^{1/2}$.) For long chains, the characteristic interfacial displacement required to separate the interface is on the order of microns. Cracks can also grow by linking of microvoids ahead of the crack tip. In elastomers, a typical stress for rapid growth of micro-voids is on the order of E ($\approx 1\,MPa$), much smaller than the stress required to break bonds. In addition, blunting of the crack tip suggests that the effective size and the thickness of the cohesive zone can be much greater than atomic dimensions. To a lesser extent, this is also true in metallic systems, where the theoretical cohesive stress based on intermolecular potential is typically much higher than the yield stress. For crazes in polymers, the thickness of the cohesive zone is typically on the order of microns. The thickness of the continuum point in the bridging zone of fiber-reinforced composites can be on the order of millimeters.

2.2. Definition of Interfacial Displacements

The discussion above shows that the thickness, H, of an interface continuum point can be much larger than m and h, which are characteristic length scales of the microstructure. The following question naturally arises: what is an appropriate definition of interfacial displacement? The inset in Fig. 1 shows two material points on opposite sides of a planar interface separated by a distance $H >> h$, sufficiently large that all deviation from bulk deformation is confined within the two points. Let $\boldsymbol{u}$ be the separation between these two material points with component u_1 normal to the interface and components u_2 and u_3 in its plane. Let $\boldsymbol{u^o}$ be the separation that would be predicted between these two points based on bulk deformation of the solids if subjected to the same remote state of stress. Then, we define the opening displacement $\boldsymbol{\delta = u\text{-}u^o}$ as the displacement of the cohesive zone and components δ_1 as the normal and δ_2, δ_3 as the slip displacements. That is, the cohesive zone displacements are the *excess relative to that which would be predicted by the bulk deformation of the solids*. (We pick H to be sufficiently large compared with h but still sufficiently small

compared with L so that stresses and strains locally are homogeneous prior to introduction of the interface and so that the displacements, so defined, are independent of the choice of H. For the special case where the interface deformation is highly localized, such as that of a craze, H can be taken to be h.)

This definition implies that the opening or slip displacements measured in the laboratory (*i.e.*, in a fracture test) can be substantially different from the opening or slip displacements used in the cohesive model. As an example, consider crazes, which are planar crack-like defects in glassy polymers. However, unlike cracks, crazes are load-bearing, since their surfaces are bridged by many fine fibrils with diameters ranging from 5 to 30 nm (see Fig. 2). As the craze grows in thickness this fibril structure may break down, leading to large voids which eventually grow to become cracks of a critical size. Experiments have conclusively demonstrated that crazes in air increase in thickness by drawing material from a thin ($\approx nm$), strain-softened layer at the craze-bulk interface into the fibrils. Since the fibril structure cannot withstand shear, $\delta_2 = \delta_3 \approx 0$. As a result, the direction of the tensile stress is always normal to the craze surface and the craze thickens primarily in the direction of its fibrils.

To illustrate the procedure of computing the interfacial displacement, δ_1, for a craze, consider Fig. 3a,b where a comparison is made between the normal displacement of two material points induced by the bulk deformation of the polymer (elastic or inelastic) and the final deformation of the same material points after the craze has formed. The separation of these two points due to homogeneous bulk deformation is denoted by H_o. The separation of these points after the craze has formed is H. Let ρ_o be the density of the homogenously deformed bulk material in Fig. 3a, and let ρ be the density of the craze and bulk

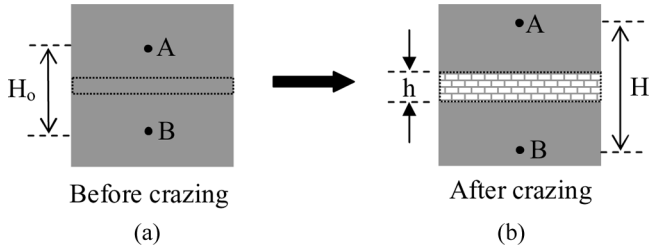

FIGURE 3 (a) Continuum point before crazing occurs. The craze material is highlighted by the dotted lines. (b) After crazing, the material inside the box highlighted in (a) increases its thickness to h and becomes less dense. The two black dots denote two points A, B before and after crazing.

material in Fig. 3b. In general, ρ is a function of the distance along the y axis (the y direction is perpendicular to the craze interface), and the planar interface is the xz-plane. Since one can reasonably assume that there is no excess lateral strain due to crazing, we have

$$\rho_o H_o = \int_0^H \rho(y)dy \equiv \bar{\rho}H \tag{1}$$

by mass conservation, where $\bar{\rho}$ is the average density of the crazed material. The interface displacement is, by definition,

$$\delta_1 \equiv H - H_o. \tag{2}$$

Substituting Eq. (1) into Eq. (2), we have

$$\delta_1 = H\left(1 - \frac{\bar{\rho}}{\rho_o}\right). \tag{3a}$$

For crazes, the craze-bulk interface is very sharp, [$\approx$10 nm, so a *convenient choice* is to select the material points so that $H = h$, where h is the visible thickness of the craze (*e.g.*, in a transmission electron micrograph]. The interface displacement is

$$\delta_1 = h\left(1 - \frac{\rho_c}{\rho_o}\right), \tag{3b}$$

where ρ_c is the average mass density in the craze[1]. *The above definition of δ_1 is independent of the distance H_o between the two material points* as long as H_o is less than L and large enough to include all the details of fibrillation. This definition is similar to an early expression of Lauterwasser and Kramer [67]. For crazes in polystyrene, $\rho/\rho_o \approx 0.2$ so that *the continuum normal displacement is about 80% of the visible craze thickness*.

In a very different application, we point out that there is some ambiguity in the published literature on the appropriate definition of interface displacement to model crack bridging in fiber-reinforced composites. As pointed out by McCartney [28], the continuum-opening displacement in the bridging model is the additional displacement of a remote material point of a cracked composite (*i.e.*, the matrix is fully

[1]Since the effective Young's modulus of the crazed material, E_c, is less than that of the bulk polymer, E, we should include the difference in elastic deformation, a factor of $h\sigma_c(E_c^{-1} - E^{-1})$ in Eq. (3b), where σ_c is the crazing stress. However, since σ_c/E is on the order of 10^{-3}, this factor is much smaller than the RHS of Eq. (3b), and so it can be neglected.

cracked) over that which would result in an uncracked composite under the same loading. This procedure is entirely consistent with our definition of interfacial displacement.

Many cohesive zone models have an initial hardening branch, that is, the interfacial displacements are non-zero for any applied traction, no matter how small. A very simple example of a linear hardening model is to consider a thin layer of soft elastic material of uniform thickness, h, perfectly bonded between two identical homogeneous, isotropic, linear elastic plates with Young's modulus, E, and Poisson's ratio, v. For simplicity, let us consider a plane stress problem (*e.g.*, a thin sheet of material between two identical plates). Let E_L and v_L denote the Young's modulus and Poisson's ratio of the layer. If h is much smaller than the crack tip radius, this layer can be treated as a cohesive zone. In the absence of the layer, the two points A, B (see Fig. 4) displace by the amount of

$$\sigma H_o/E, \tag{4a}$$

where σ is the normal stress applied at distances far from the layer (see Fig. 3). Assuming that the lateral contraction of the soft layer is the same as that of the two large identical plates, the displacement of A, B in the presence of the layer is

$$\frac{\sigma}{E}(H_o - h) + \frac{\sigma h}{E_L}\left[1 - v_L^2\left(1 - \frac{E_L v}{E v_L}\right)\right]. \tag{4b}$$

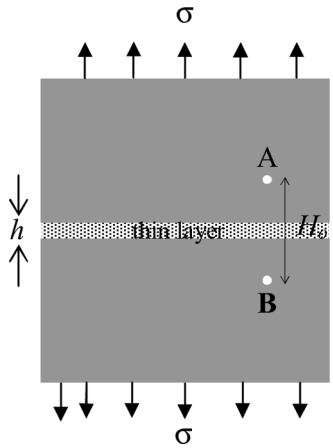

FIGURE 4 A thin elastic layer sandwiched between two linearly elastic plates.

By definition, the excess displacement or opening interface displacement, δ, is the difference between Eqs. (4b) and (4a), that is,

$$\delta = \frac{\sigma h}{E_L}\left[1 - v_L^2\left(1 - \frac{E_L v}{E v_L}\right)\right] - \frac{\sigma h}{E}. \tag{4c}$$

Note that the result is *independent* of H_o and the interface displacement *vanishes* if $E = E_L$. This simple model has a linear "hardening" branch where the interface displacement, δ, is directly proportional to the normal traction, σ. The hardening branch is typically followed by a softening branch, where σ decreases with increasing δ. The behavior of the softening branch depends on the failure characteristic of the layer. For example, if the layer fails in a brittle way (*e.g.*, by the propagation of a single crack), then softening occurs very rapidly. However, if the layer fails by cavitation[2], then the range of δ where softening occurs can be very large.

As demonstrated by the above example, our definition of interfacial displacement implies that, at least in homogeneous materials, inter-atomic models of decohesion should have no linear hardening branch since the linear elastic behavior of the continuum point is indistinguishable from the bulk behavior. However, cohesive models for the interface between two materials can have a hardening branch.

2.3. Variables in Cohesive Zone Model

The primary mechanical variables of interest are the normal traction, T_1 (traction component in the direction normal to the interface), the shear tractions T_2, T_3, and the interface displacement vector, $\vec{\delta} = (\delta_1, \delta_2, \delta_3)$ defined above. To define these displacements and tractions we need first to define a cohesive plane. *A full mechanical description could conceivably include other deformation variables such as the relative rotation of the two surfaces and the in-plane strain in the two solids.* For example, the nucleation and growth of micro-voids ahead of the crack tip can be significantly affected by the in-plane strain, especially if crack blunting occurs, since void nucleation and growth are known to be very sensitive to triaxiality. In large deformation, the traction, $\vec{T}$, should be interpreted as the Cauchy traction.

[2]Cavitation is more likely to occur if the layer were loaded in plane strain and $E >> E_L$, $\nu_L \approx 0.5$, for example, if the plates were blocks of glass and the layer were replaced by a thin sheet of rubber or soft elastic gel.

A reasonably general constitutive model for the interface or cohesive zone model can be written in the form of a relation as follows:

$$\mathsf{G}\left\{\vec{T}(t), \mathsf{F}\left[\vec{\delta}(t'), -\infty \le t' \le t\right]\right\} = 0. \tag{5a}$$

In the above, F is a vector function which depends on the history of the displacement vector that is related to the traction vector $\vec{T} \equiv (T_1, T_2, T_3)$ through the vector relation

$$\mathsf{G}\left(\vec{T}, \mathsf{F}\right) = 0. \tag{5b}$$

2.4. Definition of Cohesive Zone, Cohesive Zone Tip, and Crack Tip

The cohesive zone, cohesive zone front, and crack front can be defined in a formal way. At any time t, the cohesive zone consists of all points on the interface such that $\delta \equiv \left|\vec{\delta}\right| > 0$. A cohesive zone front is the boundary points (in general a space curve) between two adjacent regions on the interface where at least one of the interface displacements goes from identically zero in one region to having non-zero values in the other. This definition allows for multiple cohesive zone fronts within a cohesive zone and its boundaries. For example, it is possible to have part of the cohesive zone deform in a pure opening mode (or in a pure sliding mode), whereas the rest of the cohesive zone deforms in both opening and sliding mode. (An example will be given later.) In general, true cohesive zone front(s) exist only for constitutive models that allow $\delta_i = 0$ for *some* i and for some *nonzero* traction histories. In the absence of crack healing or internal fluid pressure, we define a crack zone as the part of the interface that *belongs to a cohesive zone*; however, material points in this region can bear no load for the current, and all possible future, configurations, that is $\vec{T} \equiv 0$ for all $t' \ge t$. A crack front is defined as the boundary points between a crack zone and a cohesive zone. We will illustrate these ideas shortly with some simple examples.

Although it is possible to construct examples where the displacement normal to the interface is negative (*e.g.*, a soft interface layer under compression), it is common to enforce $\delta_1 \ge 0$ at all times. In this work, we will adopt the convention that contact occurs when $\delta_1 = 0$, and friction force must be taken into account if $T_1 < 0$. *In cohesive zone models, preexisting cracks or cracks that are artificially introduced into the interface which do not satisfy a fracture criterion consistent with the cohesive zone model, cannot be considered as part of the interface and, hence, cannot be described by the model*. Descriptions of

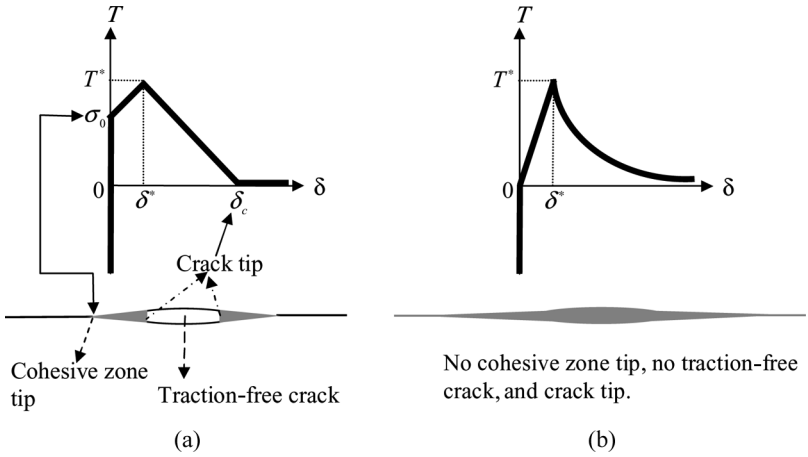

FIGURE 5 (a) A cohesive zone model where cohesive zone tips and crack tips are well defined. (b) A cohesive zone model where neither the cohesive zone tips nor crack tips exist.

these cracks must be captured by boundary conditions. We will call these types of cracks *preexisting* cracks.

Figure 5 shows some simple examples where $T_2 = T_3 = \delta_2 = \delta_3 = 0$, that is, the interface is constrained to open in the direction of its normal. The cohesive zone tip and the crack tip are well-defined for the cohesive zone model in Fig. 5a. At the cohesive zone tip, the normal traction $T = T_1$ is exactly $\sigma_0 > 0$. Crack tips are defined by the condition$\delta = \delta_c$. Note that the type of cohesive law drawn in Fig. 5a implies that within the cohesive zone is a region subjected to tractions that exceed σ_o. As pointed out by Elices *et al.* [68], adjacent regions in the bulk should also have cohesive zones. Therefore, multiple cohesive zones can exist in this model.

2.5. Constitutive Relation Based on Potential Function

A widely used constitutive relation is the reversible cohesive zone model introduced by Needleman [29,30,40]. Let a displacement $\vec{\delta} = (\delta_1, \delta_2, \delta_3)$ be imposed on a continuum point. Denote the resulting traction on this point by $\vec{T} = (T_1, T_2, T_3)$. The work done by the cohesive traction per unit area from $\vec{\delta}_a$ to $\vec{\delta}_b$ is

$$\int_{\vec{\delta}_a}^{\vec{\delta}_b} \vec{T} \cdot d\vec{\delta}. \tag{6}$$

This integral is *path-dependent* unless $\vec{T}$ is the gradient of a potential or work function $\Phi(\vec{\delta})$, *i.e.*,

$$T_i = \Phi_{,i} \quad \equiv \partial\Phi/\partial\delta_i. \tag{7}$$

Equation (7) is the fundamental equation governing the work function approach. The work function, $\Phi(\vec{\delta}) = \text{constant}$, represents a family of surfaces in the space of cohesive-opening displacements. Geometrically, Eq. (7) *states that the traction vector is normal to these equi-potential surfaces*.

An example of such a work function in two dimensions (*i.e.*, $\delta_3 = 0$) is [40]:

$$\Phi(\delta_1, \delta_2) = W_1 + W_1\left(1 + \frac{\delta_1}{\delta_1^*}\right)e^{-\frac{\delta_1}{\delta_1^*}}\left((q-1) - qe^{-\frac{\delta_2^2}{(\delta_2^*)^2}}\right), \tag{8a}$$

where $q = W_2/W_1$. W_1 is the energy needed to separate a unit area of the interface in pure tension (commonly referred to as the intrinsic work of adhesion) and W_2 is the energy needed to fail the interface in pure shear and $\delta_i^*(\mathrm{i} = 1, 2)$ are material parameters that represent characteristic distances over which the cohesive tractions act. Contour plots of this potential are shown in Fig. 6. Using Eq. (7), the traction vector is

$$T_1 = \frac{W_1\delta_1}{(\delta_1^*)^2}e^{-\frac{\delta_1}{\delta_1^*}}\left(1 - q(1 - e^{-\frac{\delta_2^2}{(\delta_2^*)^2}})\right), \tag{8b}$$

$$T_2 = \frac{2W_2\delta_2}{(\delta_2^*)^2}\left(1 + \frac{\delta_1}{\delta_1^*}\right)e^{-\frac{\delta_1}{\delta_1^*}}e^{-\frac{\delta_2^2}{(\delta_2^*)^2}}. \tag{8c}$$

The normalized tractions given by Eqs. (8b,c) are plotted in Fig. 7. A one-dimensional work function $\phi(\delta_1)$ can be extended to the three-dimensional case by defining $\Phi(\delta_1,\ \delta_2,\ \delta_3) \equiv \phi(\delta_e)$where $\delta_e \equiv \sqrt{\delta_1^2 + \beta(\delta_2^2 + \delta_3^2)}$ and $\beta > 0$ is a material constant. (In this case we assume isotropy in the interfacial plane, *i.e.*, we do not distinguish between directions "2" and "3".)

Since the failure of the interface is defined by its inability to support traction, Eqs. (8b) and (8c) imply that the interface fails if any one of the following conditions is satisfied:

i. $$\delta_1 \to \infty \tag{9a}$$

ii. $$\delta_1 = 0 \quad \text{and} \quad |\delta_2| \to \infty. \tag{9b}$$

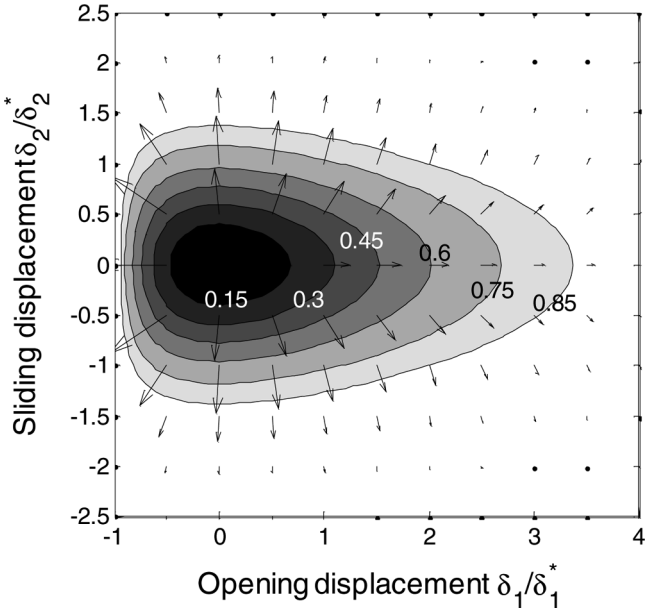

FIGURE 6 Contours of potential normalized by W_1 ($W_2 = W_1$, $q = 1$). Also shown are vectors representing tractions.

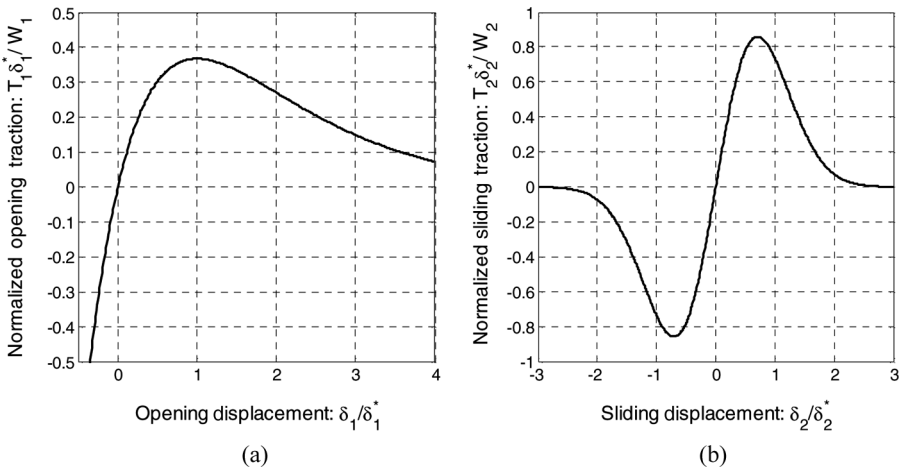

FIGURE 7 (a) Normalized opening traction $T_1\delta_1^*/W_1$ *versus* normalized opening displacement δ_1/δ_1^* when $\delta_2 = 0$; (b) Normalized sliding traction $T_2\delta_2^*/W_2$ *versus* normalized shear displacement. δ_2/δ_2^* when $\delta_1 = 0$.

Note that, unless the interface is loaded in pure shear, failure in shear must be accompanied by failure in tension.

Equations (8a–c) illustrate three features of some widely-used, potential-based, cohesive models:

1. The traction vanishes as $\vec{\delta} \to \vec{0}$ (Initial hardening, cohesive front not defined),
2. Non-zero traction for all finite $\delta \equiv \left|\vec{\delta}\right|$ (crack front not well-defined). Note that the traction vanishes much faster than δ^{-1}as $\delta \to \infty$,
3. The work to fail a unit area of the interface is always W_1, independent of the loading direction. The only exception is when the interface is loaded in pure shear. In this case the work is W_2. In the following we examine each of these features in detail.

2.6. Hardening vs. Rigid Models

Cohesive zone models in which the traction vanishes smoothly as $\vec{\delta} \to \vec{0}$ will be defined as *hardening models*. In hardening models, cohesive zone fronts can not exist in any finite structures under load (see definition of cohesive zone front earlier). In a finite element model, hardening cohesive zone models can lead to softening of bulk behavior [42,47]. Another interesting, but less well-known, result is that material interpenetration will always occur if a hardening cohesive zone model is used to study the growth of a preexisting crack loaded in Mode I. A proof of this result can be found in [69]. To the best of our knowledge, the size of this interpenetration zone at the crack tip has not been studied. It should be noted that material interpenetration is penalized in Needleman's model by the term $\delta_1 \exp(-\delta_1/\delta_1^*)$ in Eq. (5b). By making δ_1^* very small, very large normal compressive traction results as δ_1 become negative.

Thus, a cohesive zone model with a hardening branch has the following features that need to be kept in mind:

1. material softening
2. material interpenetration.

Material softening can be an issue particularly when such cohesive elements are distributed between elements throughout the mesh. If the initial hardening branch is sufficiently stiff compared with neighboring elements, material softening is less of an issue when cohesive elements lie on a single plane. Also, an initial hardening branch is beneficial for numerical implementation because cohesive elements open and close automatically and smoothly as a simulation proceeds.

By the same token, any compression borne by the cohesive interface results in interpenetration of the adjoining elements, unless additional contact constraints are applied between them.

Cohesive zone fronts are well-defined in "rigid" cohesive models such as the classical Dugdale-Barenblatt (DB) model which was used to model plane stress Mode I fracture of mild steel. This model can be extended to include shear deformation. The potential associated with the generalized Dugdale-Barenblatt (GDB) model is

$$\Phi = \sigma_o \delta_1 + \tau_o |\delta_2| + \tau_o |\delta_3|, \tag{10}$$

where σ_o, τ_o are the critical cohesive stresses to open and slip the interface, respectively. To prevent material interpenetration, the potential function is defined in the half space $\delta_1 > 0$. According to Eqs. (6) and (8), interface displacements can occur if

$$T_1 = \sigma_o \quad \delta_1 > 0, \tag{11a}$$

$$T_i = \pm\tau_o \quad \delta_i > 0(+), \delta_i < 0(-),\ i = 2, 3. \tag{11b}$$

In analogy with classical plasticity, the planes $T_1 = \sigma_o$ and $T_i = \pm\tau_o$ can be viewed as a "yield" surface in traction space (T_1, T_2, T_3). A traction vector that is inside the yield surface cannot cause interfacial displacement. Note that the origin $\vec{\delta} = \vec{0}$ is a point where the traction vector is not uniquely defined. Also, the GDB model yield surface is not smooth; it has corners at the vertices of the rectangle defined by the intersections of the lines in Eqs. (11a,b).

Specifically, a rigid cohesive model must formally satisfy the condition

$$\lim_{\vec{\delta} \to \vec{0}^+} \vec{T} \neq \vec{0}. \tag{12}$$

The notation $\vec{\delta} \to 0^+$ implies that the limit is taken with $\delta \equiv \left|\vec{\delta}\right| > 0$. Note that $\lim_{\vec{\delta} \to \vec{0}} \vec{T}$ does not exist in the usual mathematical sense since the traction vector is not a continuous function of the interface displacement vector at zero. In this work, the existence of $\lim_{\vec{\delta} \to \vec{0}} \vec{T}$ means that the traction vector will approach a unique value *given any smooth path approaching the origin in displacement space with* $\delta > 0$, although each path will, in general, produce a different limit. We further assume that this limit depends only on the tangent of the path as it approaches $\delta = 0$; in other words, *the limiting value of traction is the same for all smooth curves entering* $\delta = 0$ *with the same slope.* The resulting potential surface defined by this limiting process in stress space is called a yield surface, in analogy with classical plasticity. For a perfectly rigid cohesive zone model, the traction vector must lie inside or on the yield surface. The interface displacement vector is identically

zero for any traction vector inside the yield surface. Plastic flow is equivalent to the motion of the interface. Equation (7) implies that interface motion in a rigid cohesive zone model is possible if, and only if, the traction vector is normal to equi-potential surfaces in displacement space.

For example, suppose that the potential function is given by:

$$\Phi = A\sqrt{\delta_1^2 + \beta(\delta_2^2 + \delta_3^2)}, \qquad \beta > 0, \tag{13}$$

where A and β are positive constants. For non-trivial displacement, the traction is

$$\vec{T} = \frac{A}{\sqrt{\delta_1^2 + \beta(\delta_2^2 + \delta_3^2)}}(\delta_1, \beta\delta_2, \beta\delta_3). \tag{14}$$

This model is perfectly rigid since the limit of $\vec{T}$ as $\vec{\delta} \to \vec{0}$ is in general a non-zero vector (see below). Furthermore, Eq. (14) implies that

$$A^{-2}T_1^2 + \left(A^2\beta\right)^{-1}(T_2^2 + T_3^2) = 1. \tag{15}$$

Equation (15) implies that the yield surface is an ellipsoid of revolution with semi-axis $A$and $A\sqrt{\beta}$. For the special case of$\beta = 1$, the yield surface is a sphere of radius A. A path in displacement space corresponds to a path on the yield surface. For example, consider a straight line path $\delta_2 = a\delta_1$, $\delta_3 = b\delta_1$ in displacement space, where *a, b* are positive numbers. The image of this path on the yield surface can be obtained using Eq. (14). For this special case, the path in stress space collapses to a single point on the yield surface, *i.e.*, $\vec{T} = \frac{A}{\sqrt{1+\beta(a^2+b^2)}}\ (1, \beta a, \beta b)$. Thus, the interface continues to deform under this constant traction, in analogy with a rigid plastic material.

In general, it is possible to construct rigid models in which the yield surface evolves with interface motion. For example, consider

$$\Phi = \sqrt{\delta_1^2 + \beta(\delta_2^2 + \delta_3^2)}\chi(\delta_1, \delta_2, \delta_3), \tag{16}$$

where χ is a smooth function of its arguments. In particular, $\chi(0, 0, 0) = A > 0$. For this case, the initial yield surface is still given by Eq. (15), but subsequent yield surfaces are determined by the behavior of χ. As an example, consider

$$\Phi = \sqrt{\delta_1^2 + \beta(\delta_2^2 + \delta_3^2)}e^{-\delta_1 - (\delta_2^2 + \delta_3^2)}. \tag{17}$$

Equation (17) implies that the yield surface shrinks with interfacial motion. It can be verified easily that the traction decreases with the

size of the yield surface and that failure of the interface occurs when the yield surface shrinks to the point $\vec{\delta} = \vec{0}$.

It is well known that the interface fracture toughness of bimaterial systems is dependent on the applied phase angle, see for example [70,71]. Potential functions that satisfy condition 3 [see paragraph after Eq. (9b)] in general can not predict such dependence, unless the material outside the cohesive zone undergoes inelastic deformation. In this case, the size of the plastic zone depends on both the cohesive model and the plastic flow rule. As a result, the energy dissipated as the crack advances depends on the loading direction, even though the intrinsic work to separate the interface does not. This approach has been pursued by Tvergaard and Hutchinson [36,37]. The relationship between toughness, fracture strength, and the intrinsic work of adhesion in [36] can actually be captured by a cohesive model which represents the two-dimensional plastic flow in the crack tip region by a set of one-dimensional inelastic springs [72]. However, there are many physical systems where inelastic deformation is primarily confined to a thin layer of material along interfaces, for example, friction sliding, shear deformation zone in polymers, and adhesive failure of lap joints. Furthermore, there is no intrinsic reason which suggests that the work to fail an interface must be independent of the loading direction. For example, the experimental data of Yang *et al.* [52] showed significant differences in Mode I and Mode II toughness.

It is not difficult to construct potentials with directional interfacial fracture energies. For example, consider the potential

$$\Phi(\delta_1, \delta_2) = W_{II} \tanh\left(\frac{\alpha\bar{\delta}_1^2 + \bar{\delta}_2^2}{1 + \bar{\delta}_1^2}\right), \tag{18}$$

where α is defined by $\tan h\alpha \equiv W_I/W_{II}$. Contour plots of the potential given by Eq. (18) are shown in Fig. 8. In Eq. (18), the displacements are normalized by some appropriate characteristic length δ^*, *i.e.*, $\bar{\delta}_i = \delta_i/\delta^*$. Note

$$\Phi(\delta_1 = 0, \delta_2 \to \infty) = W_{II} \tag{19a}$$

$$W_I \equiv \Phi(\delta_1 \to \infty, \delta_2 = 0) = (\tanh\alpha) W_{II} = W_I \tag{19b}$$

For proportional loading in displacement space, *i.e.*, if $\delta_1 \to \infty$ and $\delta_2 \to \infty$ along the line $\delta_1/\delta_2 = b$, then

$$\Phi(\delta_1 \to \infty, \delta_2 \to \infty) = W_{II} \tanh\left(\frac{\alpha b^2 + 1}{b^2}\right). \tag{20}$$

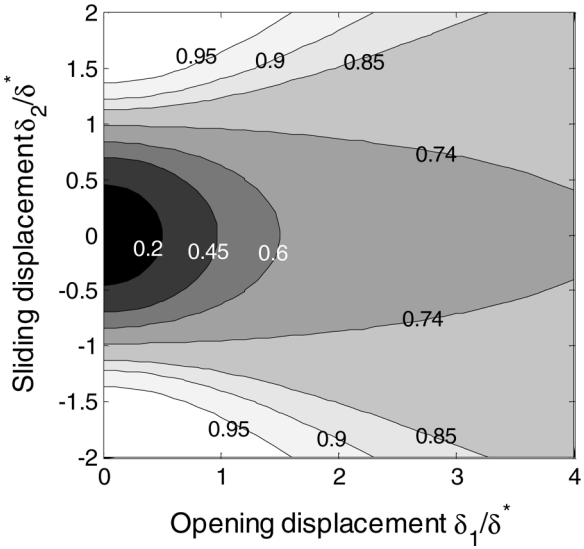

FIGURE 8 Contours of normalized potential (Φ/W_{II}) as a function of normalized opening displacement $\bar{\delta}_1$ and sliding displacements $\bar{\delta}_2$.

The tractions are:

$$T_1 = W_{II}\frac{2\bar{\delta}_1\left(\alpha-\bar{\delta}_2^2\right)}{\delta_*\left(1+\bar{\delta}_1^2\right)^2}\operatorname{sech}^2\left(\frac{\alpha\bar{\delta}_1^2+\bar{\delta}_2^2}{1+\bar{\delta}_1^2}\right), \tag{21a}$$

$$T_2 = W_{II}\frac{2\bar{\delta}_2}{\delta_*\left(1+\bar{\delta}_1^2\right)}\operatorname{sech}^2\left(\frac{\alpha\bar{\delta}_1^2+\bar{\delta}_2^2}{1+\bar{\delta}_1^2}\right). \tag{21b}$$

Equations (21a,b) imply that if $\delta_1 \to \infty$ and $\delta_2 \to \infty$ along the line $\delta_1/\delta_2 = b$, the magnitude of the traction vanishes like $|\vec{T}| \approx 1/\delta$, where $\delta \equiv \sqrt{\delta_1^2+\delta_2^2}$. In general, the work to fail a unit area of the interface depends on the rate for which $\delta_1 \to \infty$ and $\delta_2 \to \infty$. For example, if $\delta_1 = \beta\delta_2^2$ and $\delta_2 \to \infty$, then

$$\Phi(\delta_1 \to \infty, \delta_2 \to \infty) = W_I. \tag{22}$$

We now show that the traction associated with potentials which allow directional fracture energies must decay like δ^{-1} as$\delta \to \infty$. To demonstrate this result, we employ a polar description of the work function, *i.e.*, $\Phi = \Phi(\delta,\ \theta)$, where $\delta \equiv \sqrt{\delta_1^2+\delta_2^2}$ and $\theta \equiv \tan^{-1}(\delta_2/\delta_1)$.

In polar coordinates, the tractions are

$$T_\delta = \partial\Phi/\partial\delta,\ T_\theta = \frac{1}{\delta}\frac{\partial\Phi}{\partial\theta}. \tag{23}$$

$(T_\delta,\ T_\theta)$ is related to $(T_1,\ T_2)$ by usual vector transformation:

$$T_\delta = T_1\cos\theta + T_2\sin\theta, \quad T_\theta = (-T_1\sin\theta + T_2\cos\theta). \tag{24}$$

The displacement $(\delta_\delta,\ \delta_\theta)$ is related to $(\delta_1,\ \delta_2)$ by a similar expression. The requirement that the fracture toughness depends on the loading direction implies that $\Phi(\delta\to\infty,\ \theta)\to G(\theta)$. Therefore, a necessary condition for the work function to have different interfacial energies for different loading directions is $dG/d\theta \neq 0$. If this is the case, then Eq. (23) implies that T_θ must vary as δ^{-1} as $\delta\to\infty$. Another way to understand this result is to note that the work done by the traction from $\vec{\delta}_a$ to $\vec{\delta}_b$ is

$$\Phi_{ab} = \int_{\vec{\delta}_a}^{\vec{\delta}_a} (T_R d\delta_R + T_\theta d\delta_\theta). \tag{25}$$

Let $\vec{\delta}_a$ and $\vec{\delta}_b$ lie on a very large circle with radiusδ. Since $G(\theta)$ is a non-constant function, Φ_{ab} cannot be zero. Since $\vec{\delta}_a$ and $\vec{\delta}_b$ lie on a circular path, $d\delta_R = 0$ and $d\delta_\theta = \delta d\theta$. This implies that $\Phi_{ab} = \delta\int_{\theta_a}^{\theta_b} T_\theta d\theta$. Thus, for bounded non-zero values of Φ_{ab}, $T_\theta \propto 1/\delta$ as $\delta\to\infty$. Also, the first equation in Eq. (23) implies that T_δ must decay faster than $1/\delta$ as $\delta\to\infty$. This result, together with Eq. (24), shows that T_1, T_2 vanishes as $1/\delta$ as $\delta\to\infty$.

Why don't we use this type of potential? The problem is that potentials with directional dependent interface energies always violate steady state crack growth under small scale yielding (SSY) conditions. To see this, consider a semi-infinite plane strain crack lying along the negative real axis. The material is assumed to be homogeneous, isotropic, and linearly elastic with Young's modulus E. The SSY boundary condition is

$$\sigma_{ij}(r\to\infty,\theta) = \frac{K_I}{\sqrt{2\pi r}}f_{ij}^I(\theta) + \frac{K_{II}}{\sqrt{2\pi r}}f_{ij}^{II}(\theta), \tag{26}$$

where $(r,\ \theta)$ is a polar coordinate system at the crack tip. $f_{ij}^I(\theta)$ and $f_{ij}^{II}(\theta)$ are universal dimensionless functions describing the angular variation of the stresses. To satisfy SSY, the stresses due to the cohesive zone must be small compared to the applied field (26) as

$r \to \infty$. SSY and steady state crack growth implies that interfacial displacement in the far field must be given by

$$\delta_1 \propto K_I\sqrt{-x}/E \quad \text{and} \quad \delta_2 \propto K_{II}\sqrt{-x}/E \quad \text{as} \quad x \to -\infty. \tag{27}$$

On the other hand, our previous analysis shows that T_θ is proportional to $1/\sqrt{\delta_1^2 + \delta_2^2}$ *as* $\sqrt{\delta_1^2 + \delta_2^2} \to \infty$. According to Eq. (27), T_θ *must vary as* $1/\sqrt{-x}$ *as* $x \to -\infty$. *This would mean that the normal cohesive traction is of the same order of magnitude as the applied stresses at infinity—a contradiction to the assumption of SSY.*

Thus, potentials defined in the half space $\delta_1 > 0$ with direction-dependent interfacial energies are inconsistent with SSY. This is a very undesirable feature given the fundamental importance of the separation of length scales represented by SSY in fracture. To develop cohesive zone models capable of predicting mixed mode failure in *elastic* materials, at least two other choices are possible. The first is to supplement the work function approach with the concept of failure surface in displacement space, as discussed below. The basic idea of this approach is similar to a model developed earlier by Yang and Thouless [73]. The second choice is to consider non-potential constitutive models.

3. ANISOTROPIC FAILURE SURFACE

To motivate the concept of an anisotropic failure surface, consider the classical one-dimensional DB model where the cohesive traction is the gradient of the potential $\Phi = \sigma_o\delta_1$. Note that the potential is *unbounded* as $\delta_1 \to \infty$. The cohesive traction, σ_o, is independent of the opening displacement and hence does not vanish as $\delta_1 \to \infty$. Failure of the interface is defined by imposing the ***additional*** condition $\delta_1 = \delta_c$, where δ_c is the critical crack opening displacement.

This idea can be readily extended to the multi-axial loading case by defining the work to fail an interface by

$$\int_0^{\vec{\delta}_c} \vec{T} \cdot d\vec{\delta}, \tag{28a}$$

where $\vec{\delta}_c$ is a vector which lies on a closed surface, $\partial\Omega$, in the displacement space (δ_1, δ_2, δ_3). This surface is defined as the failure surface and it is assumed to be closed and bounded. In addition, the origin $\vec{\delta} = \vec{0}$ is assumed to lie in its interior Ω. The traction, $\vec{T}$, is still given

by the gradient of a work function, but the domain of the work function is now restricted to Ω. Since the work function is defined in an open set, the work function has no meaning once the material has failed. In other words, points on the failure surface cannot be reached by loading paths which lie on or outside the failure surface. Once the failure surface is reached, the traction on the interface is set to zero, *i.e.*,

$$\vec{T} = \vec{0}, \qquad \vec{\delta} \in \partial\Omega \tag{28b}$$

As an example, consider the special case of a two-dimensional problem where $\delta_3 = 0$ and the failure surface is defined by the ellipse

$$\delta_{1c}^2 + c^2\delta_{2c}^2 = \delta_c^2, \tag{29}$$

where δ_{1c} and δ_{2c} are the opening and slip displacements at the tip of a pre-existing crack, $0 < c < 1$, and δ_c is a material constant. Let us assume the potential is given by Eq. (8a). For simplicity, we set $\delta_1^* = \delta_2^* = \delta_c$ in Eq. (8a). In addition, we consider $W \equiv W_1$ and $q > 1$ as parameters. The domain of the work function

$$\Phi(\delta_1, \delta_2) = W + W\left(1 + \frac{\delta_1}{\delta_c}\right)e^{-\delta_1/\delta_c}\left((q-1) - qe^{-\delta_2^2/\delta_c^2}\right) \tag{30}$$

is the interior of the ellipse Eq. (29). By definition, the work, W_I to fail a unit area of the interface in the opening mode is computed using Eqs. (29) and (30), *i.e.*,

$$W_I = \Phi(\delta_1 = \delta_{1c} = \delta_c, \delta_2 = 0) = W\left[1 - 2e^{-1}\right]. \tag{31a}$$

Similarly, failure in pure sliding mode occurs when $\delta_1 = 0$; $\delta_2 = \delta_{2c} = \delta_c/c$. Equations (29) and (30) imply that

$$W_{II} = q(1 - e^{-1/c^2})W. \tag{31b}$$

For sufficiently large q and small c, the ratio W_{II} / W_I can be arbitrarily large.

Let us use this model to study the fracture of a pre-existing plane strain crack in a linear isotropic elastic material with Young's modulus, E, and Poisson's ratio, ν, under SSY conditions. The crack tip is located at the origin with the crack occupying the negative real

axis. The maximum opening and sliding displacements in the cohesive zone occur at the crack tip and are completely determined by the applied stress intensity factors, K_I and K_{II}. Dimensional analysis implies that these displacements have the following form:

$$\delta_{1c} = \frac{K_I^2}{E^* \sigma_o} f_1(K_{II}/K_I), \tag{32a}$$

$$\delta_{2c} = \frac{K_I^2}{E^* \sigma_o} f_2(K_{II}/K_I), \tag{32b}$$

where $E^* = E/(1-\nu^2)$, $\sigma_o \equiv W/\delta_c$, and f_i are unknown dimensionless functions. These dimensionless functions can be determined using numerical methods. Since fracture occurs when Eq. (29) is satisfied, Eqs. (32a,b) imply that

$$\left(\frac{K_I^2}{E^* \sigma_c}\right)^2 [f_1(K_{II}/K_I)]^2 + c^2 \left(\frac{K_{II}^2}{E^* \sigma_c}\right)^2 [f_2(K_{II}/K_I)]^2 = \delta_c^2. \tag{33}$$

Once the f_i's are determined, Eq. (33) completely specifies the failure locus in (K_I, K_{II}) or K space. Thus, there is a one-to-one correspondence between the failure surface in the displacement space and the failure surface in K space. Clearly, the failure surface described by Eq. (33) is anisotropic. It is interesting to note that an equivalent form of Eq. (33) can be obtained using the energy balance. Indeed, at the onset of fracture, the energy release rate must equal to the work of adhesion, *i.e.*,

$$\frac{(K_I^2 + K_{II}^2)}{E^*} = W + W\left(1 + \frac{\delta_{1c}}{\delta_c}\right) e^{-\delta_{1c}/\delta_c} \left((q-1) - q e^{-\frac{(\delta_c^2 - \delta_{1c}^2)}{c^2 \delta_c^2}}\right), \tag{34}$$

where δ_{1c} is given by Eq. (32a). Equations (33) and (34) are equivalent and they predict the same failure locus in K space.

In general, the failure locus in displacement space is a curve described by

$$F(\delta_{1c}, \delta_{2c}) = 0. \tag{35}$$

This curve intersects the positive δ_1 axis at δ_{cod}, the displacement for the interface to fail in the opening mode. For an isotropic interface, this curve also intersects the δ_2 axis at $\pm\delta_{csd}$, the critical shear displacements under pure sliding. The work to fail the interface in pure opening mode and sliding mode is given by $\Phi(\delta_{cod}, 0) = W_I$

and $\Phi(0, \pm\delta_{csd}) = W_{II}$, respectively. Once the potential and the failure surface are specified, the failure surface in K space is determined by solving a mechanics problem. In general, the failure surface in K space is anisotropic so that this theory is capable of predicting mixed mode fracture in elastic materials. In this approach, cohesive tractions will generally jump abruptly to zero as one traverses the crack front, as is the case in the Dugdale model. An example of this approach can be found in the recent work of Park *et al.* [74].

3.1. Multiple Cohesive Zone Fronts

Rigid cohesive zone models can have multiple cohesive zone tips, as illustrated by the following example. Consider the generalized DB cohesive zone model described by Eqs. (10) or (11a,b). Let us consider a *pre-existing* plane strain crack lying along a bimaterial interface which coincides with the x-axis. The region of slip and opening along the interface is assumed to be small compared with the crack length so that the crack can be considered to be semi-infinite. The crack lies along the negative x axis and with its tip at $x = -a$, $a > 0$. SSY implies that the far field interface traction is given by

$$\lim_{x\to\infty, y=0} T_1 + iT_2 = \frac{K_1 + iK_2}{\sqrt{2\pi x}} e^{-i\varepsilon}, \tag{36}$$

where $K_1 + iK_2$ is the complex stress intensity factor and ε is the oscillation index of the bi-material elastic system [75]. For simplicity, we consider the special case of $\varepsilon = 0$ which corresponds to the case of a homogeneous material or an incompressible linear elastic solid bonded to a rigid substrate. Let the tip of the shear cohesive zone be located at the origin $x = 0$. Without loss in generality, assume the opening zone is shorter than the sliding zone so that the opening zone tip is at $x = -b$, $a > b > 0$. The length of the opening zone is $L_o = a - b$ and the length of the slip zone, L_s, is a. It can be shown that [76]

$$L_s = a = \frac{\pi}{8}\left(\frac{K_{II}}{\tau_o}\right)^2, \tag{37}$$

$$L_o = a - b = \frac{\pi}{8}\left(\frac{K_I}{\sigma_o}\right)^2. \tag{38}$$

The cohesive zone tips coincide if, and only if, $L_o = L_s$ or

$$\left(\frac{K_{II}}{\tau_o}\right)^2 = \left(\frac{K_I}{\sigma_o}\right)^2. \tag{39}$$

This result shows that multiple cohesive zone tips will occur unless the applied mode mixity is $|\tau_o/\sigma_o|$. Note that Eq. (39) is valid even if σ_o is a function of τ_o. The maximum crack opening and sliding displacements at $x = -a$ are

$$\delta_{1c} = \frac{K_I^2}{E^*\sigma_o}, \quad \delta_{2c} = \frac{K_{II}^2}{E^*\tau_o}, \tag{40}$$

respectively.

The failure locus in K space is obtained by specifying an anisotropic failure curve in displacement space. For example, suppose the failure curve is given by Eq. (29), then the failure locus in K space is obtained by substituting Eq. (40) in Eq. (29), resulting in

$$\left(\frac{K_I^2}{E^*\sigma_o}\right)^2 + c^2\left(\frac{K_{II}^2}{E^*\tau_o}\right)^2 = \delta_c^2. \tag{41}$$

The fracture energy to fail a unit area of the interface, W, depends on the loading direction. W is related to the cohesive parameters and the crack opening displacement via the work function defined by Eq. (10), *i.e.*,

$$W = \sigma_o\delta_{1c} + \tau_o|\delta_{2c}| = \sigma_o\delta_{1c} + \tau_o\sqrt{\delta_c^2 - \delta_{1c}^2}/c. \tag{42}$$

For example, the work to fail a pure Mode II crack is, according to Eq. (42):

$$W_{II} = \tau_o\delta_c/c = \tau_o\sigma_o\delta_c/(\sigma_o c) = c^{-1}(\tau_o/\sigma_o)W_I. \tag{43}$$

Note that $W_{II} > W_I$ if $\tau_o/\sigma_o > c$.

3.2. Condition for Multiple Cohesive Zone Fronts

Since cohesive zone fronts are defined only for rigid cohesive models, multiple fronts can only exist for these models. First, consider smooth potential functions, Φ. Assuming an isotropic interface, symmetry considerations imply that there can be no shear traction in pure opening

mode[3], *i.e.*,

$$\partial\Phi/\partial\delta_2|_{\delta_2=0,\delta_1\to 0^+} = T_2(\delta_2 = 0, \delta_1 \to 0^+) = 0. \tag{44a}$$

We further make the reasonable assumption that there can be no normal traction in pure slip mode, that is,

$$\partial\Phi/\partial\delta_1|_{\delta_1=0,\delta_2\to 0^+} = T_1(\delta_1 = 0, \delta_2 \to 0^+) = 0. \tag{44b}$$

Based on these assumptions, we establish a condition for the existence of multiple fronts. Consider the following two-dimensional problem where a *pre-existing* semi-infinite crack lies on the x-axis. Assume a far field loading given by Eq. (36); thus, both shear and normal stresses are non-zero directly ahead of the crack tip. Consider first the case where a multiple cohesive tip exists in which $\delta_1 = \delta_2 = 0$ for $x > 0$ and $\delta_2 = 0$ $\delta_1 > 0$ in $(-s, 0)$ for some $s > 0$. Let T_1 and T_2 denote the shear and normal interface stress ahead of the cohesive tip, *i.e.*, $x \geq 0$, $y = 0$. These stresses are non-zero and *continuous* everywhere on the x axis, in particular, $T_2 \neq 0$ at $x = 0$. However, since $T_2 \neq 0$, continuity implies that $\partial\Phi/\partial\delta_2|_{\delta_2=0,\delta_1\to 0^+} \neq 0$; this contradicts Eq. (44a), so multiple tips where opening occurs before slip (tip of slip zone behind opening zone tip) cannot exist. To satisfy $T_2(x = 0) \neq 0$ and $T_1(x = 0) \neq 0$, the displacement δ_1, δ_2 must approach zero at an angle with absolute value greater than 0 and less than 90 degrees [*i.e.*, $\delta_2 \to 0^+$, $\delta_1 \to 0^+$, $|\delta_2|/\delta_1 > 0$, see discussion after Eq. (12)], that is, *both* open and slip displacement must occur together at $x = 0$. In particular,

$$T_2(x = 0) = \partial\Phi/\partial\delta_2|_{\delta_2\to 0^+,\delta_1\to 0^+,|\delta_2|/\delta_1>0}. \tag{45a}$$

An example of Eq. (45a) is the potential function specified by Eq. (13). For this case, Eq. (14) implies that

$$\partial\Phi/\partial\delta_2|_{\delta_2=0,\delta_1\to 0^+} = 0, \tag{45b}$$

but $\partial\Phi/\partial\delta_2|_{\delta_2\to 0,\delta_1\to 0^+} \neq 0$; its value depends on how δ_1 *and* δ_2 *approach zero.*

Similarly, consider the other situation where slip occurs before opening. This corresponds to $\delta_1 = \delta_2 = 0$ for $x > 0$ and $\delta_1 = 0$, $\delta_2 > 0$ in $(-s, 0)$ for some $s > 0$. As one approaches $x = 0$ from $x > 0$, the traction vector enters the initial yield surface. However, since $T_1 \neq 0$,

[3]For small δ_2, the shear traction is an odd function of δ_2. Anisotropy can develop for larger values of δ_2.

continuity implies that $\partial\Phi/\partial\delta_1|_{\delta_1=0,\delta_2\to 0^+} \neq 0$; this contradicts Eq. (44b), so multiple front of the above form also cannot exist.

On the other hand, potential functions such as the generalized Dugdale-Barenblatt model have corners on the δ_1-, δ_2- and δ_3-axis. Figure 9a shows the equi-potential line $\Phi = a > 0$ for the generalized Dugdale-Barenblatt model in the (δ_1, δ_2) plane. Note that since we are interested in the behavior near the cohesive zone tip, $a << 1$. The gradient of the potential function, Φ, is not defined at the corner on the δ_1-axis and the two corners on the δ_2-axis. The resulting traction at this point, which corresponds to a pure opening mode, can be any vector with $T_1 = \sigma_o$ and $T_2 \in (-\tau_0, \tau_0)$, *i.e.*, in between the two dashed arrows onδ_1-axis in Fig. 9a. In other words, any traction vector with $T_1 = \sigma_o$ that lies inside this wedge of internal angle $2\tan^{-1}(\sigma_o/\tau_o)$ can cause the interface to open with zero slip. Likewise, notice that the slope of the equi-potential line at ($\delta_1 = 0$, $\delta_2 = a/\tau_0$) is $-\sigma_0/\tau_0 \neq 0$. This feature implies that in a pure shear mode, the traction can be any vector with $T_2 = \tau_0$ and $T_1 \in (0, \sigma_0)$. Therefore, the generalized Dugdale-Barenblatt model violates Eqs. (44a,b) and can admit multiple cohesive fronts. In contrast, the equi-potential curve $\Phi = a > 0$ of the work function given in Eq. (13) is shown in Fig. 9b. Note that this curve has no corners and satisfies Eqs. (44a,b). Finally, our analysis shows that multiple cohesive zone fronts can exist for smooth

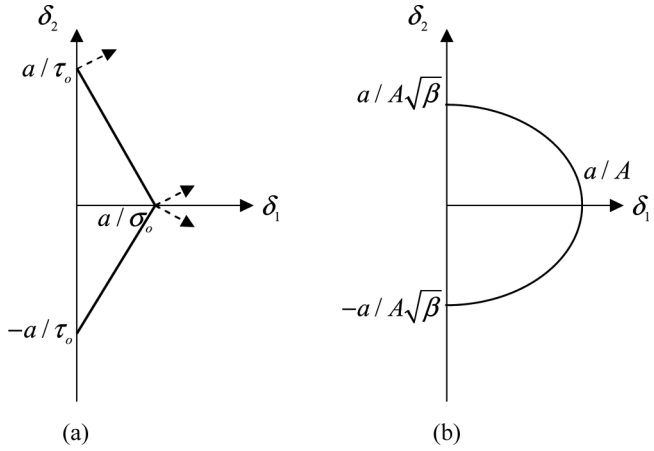

FIGURE 9 (a) An equi-potential surface of the generalized Dugdale-Barenblatt model formed by the lines $\delta_1 = 0$, $\sigma_o\delta_1 \pm \tau_o\delta_1 = a$. (b) An equi-potential surface of the work function given in Eq. (13) in the (δ_1, δ_2) plane. *Note*: Since we are interested in the behavior near the tip, $a \to 0$.

cohesive zone models that violate Eqs. (44a,b), *i.e.*, interfaces that are anisotropic even in their virgin states.

4. HISTORY DEPENDENT INTERFACE

A general approach to describe constitutive behavior of interfaces is to consider rate-dependent state-variable models. A general form of this model is

$$T_i = f_i(\dot{\delta}_1, \dot{\delta}_2, \dot{\delta}_3, \phi_1, \phi_2 ..... \phi_m), \quad i = 1, 2, 3, \tag{46a}$$

$$\dot{\phi}_j = h_j(\dot{\delta}_1, \dot{\delta}_2, \dot{\delta}_3, \phi_1, \phi_2 ..... \phi_m). \tag{46b}$$

A state is a point in the state space, consisting of tuples of the form(δ_1, δ_2, δ_3, ϕ_1, $\phi_2 ..... \phi_m$), where δ_1, δ_2, δ_3, ϕ_1, $\phi_2 ..... \phi_m$ are state variables. If the history of δ_1, δ_2, δ_3 is given, then the evolution of the interface traction (T_1, T_2, T_3) and the state variables ϕ_j can be computed by solving Eqs. (46a,b) with initial data. In this case the tractions are not necessarily derived from a potential.

For concreteness, we restrict our attention to a one-state variable theory. Without loss of generality, we consider the two-dimensional problem where $\delta_3 = 0$. There is no theoretical difficulty extending the following derivation to include multi-state variables and the out-of-plane displacement.

We demonstrate that state variable equations of the form Eqs. (46a,b) can be reduced to rate-independent interface models capable of predicting mixed mode fracture. In the rate-independent limit, the interface tractions are independent of the magnitude of the displacement rates. In other words, the functions f_i must be invariant to the transformation $\dot{\delta}_i \to a\dot{\delta}_i$, where$a > 0$. Furthermore, $\dot{\phi} \to a\dot{\phi}$ upon such a transformation. Mathematically, we must have

$$f_i(\phi, \dot{\delta}_1, \dot{\delta}_2) = f_i(\phi, a\dot{\delta}_1, a\dot{\delta}_2) \quad \forall a > 0 \tag{47a}$$

and

$$h(\phi, a\dot{\delta}_1, a\dot{\delta}_2) = ah(\phi, \dot{\delta}_1, \dot{\delta}_2) \quad \forall a > 0. \tag{47b}$$

Equation (47a) shows that, if $\dot{\delta}_1, \dot{\delta}_2$ are changed to $R = \sqrt{\dot{\delta}_1^2 + \dot{\delta}_2^2}, \theta = \tan^{-1}(\dot{\delta}_2/\dot{\delta}_1)$, then in the rate-independent limit, the functions f_i must be independent of R. Therefore, in this limit, the traction is related to the state variable and the displacement rates by

$$T_i = f_i(\phi, \tan^{-1}(\dot{\delta}_2/\dot{\delta}_1)). \tag{48}$$

Equation (47b) implies that

$$ah(\phi,R,\theta) = h(\phi,aR,\theta) \Leftrightarrow h(\phi,R,\theta) = RH(\phi,\theta). \tag{49}$$

Equations (46b) and (49) imply that, in the rate independent limit, the rate of change of the state variable must have the form

$$\dot{\phi} = \sqrt{\dot{\delta}_1^2 + \dot{\delta}_2^2} H(\phi, \tan^{-1}(\dot{\delta}_2/\dot{\delta}_1)). \tag{50}$$

For the rest of this paper, we will focus on rate-independent plasticity-like interface models. These models address the fact that most interfacial processes are irreversible; as a result, the unloading behavior of such interfaces cannot be captured by potential-based models. The rate-independent models proposed below are expected to be applicable to materials where the bulk response is represented well by rate-independent plasticity models. It can potentially be applied to study problems such as fatigue crack growth in metals and polymeric materials.

4.1. Damage-Based Interface Models

The rate-independent formulation above is quite general. In this section we give examples of models which obey Eqs. (48) and (50).

Ortiz and Suresh [49] and Camacho and Ortiz [44] introduced rate-independent, damaging and irreversible, cohesive zone models. Ortiz and Suresh [49] employed a linear cohesive model that fails at a critical value of opening traction, thus rendering their work of fracture strongly dependent on mode mixity, diverging to infinity at phase angle of $\pi/2$. Camacho and Ortiz [44] added cohesive elements adaptively as the crack propagated. They used a mixed-mode, traction-based criterion for introduction of a cohesive element, *e.g.*, under tension,

$$\sigma^{eff} = \sqrt{\sigma^2 + \beta\,\tau^2} > \sigma_{fr} \quad (\sigma > 0) \tag{51a}$$

Note that Eq. (51a) is in the form of Eq. (15) and so the corresponding potential in our notation can be obtained by using Eqs. (13) and (14). Cohesive tractions were assumed to weaken irreversibly with increasing opening. Under tension, for example, the critical tensile traction is reduced as

$$\sigma_{fr} = \sigma_o\left(1 - \frac{\delta}{\delta_{cr}}\right), \tag{51b}$$

where δ is the maximum opening experienced and δ_{cr} is the value of the state variable at which the interface loses its ability to support

tractions. If tractions on the interface are reduced below the current value of σ_{fr} at any time prior to complete separation, unloading is assumed to be linear, reversible, and through the origin. In our notation, this can be written as

$$\dot{\phi} = \dot{\sigma}_{fr} = -\sigma_o \frac{\dot{\delta}_1}{\delta_{cr}} = -\frac{\sigma_o}{\delta_{cr}} \frac{\sqrt{\dot{\delta}_1^2 + \dot{\delta}_2^2}}{\sqrt{1 + \dot{\delta}_2^2/\dot{\delta}_1^2}} HS\left(\dot{\delta}_1\right) HS(\phi); \quad \phi(0) = \sigma_o, \tag{51c}$$

and $HS(x)$ is the step function.

By combining the cohesive elements with a sophisticated finite element scheme for solving coupled, multi-body mechanics and dynamics, Camacho and Ortiz [44] show dramatic capability of cohesive zone models when interspersed between all elements, to produce multiple cracks, crack branching, fragmentation, etc. Finite elements that incorporate cohesive zone models are now available in commercial finite element codes [77]. The cohesive zone can be modeled either as a continuum (finite-thickness and continuum material properties), or using a traction-separation law (infinitesimal-thickness). In the former case, the model is only slightly different from a conventional finite element simulation with some regions of thin adhesive. In the latter case, the current implementation in ABAQUS® [77], based on [78,79], assumes progressive damage and cannot be used for crack-healing, for example.

4.2. Rate Independent Plastic Interface Model: No Initial Hardening

We first consider interface models that have *no hardening* behavior. We introduce the concept of an initial yield surface. As in classical plasticity, all admissible interface traction (T_1, T_2) must lie inside or on an initial yield surface in traction space. We denote this surface by

$$F(T_1, T_2) = C. \tag{52a}$$

An example of an initial yield surface is:

$$F(T_1, T_2) = (T_1/\sigma_c)^2 + (T_2/\tau_c)^2 = 1, \tag{52b}$$

where σ_c, τ_c are the interfacial tensile and shear strength, respectively. The existence of an initial yield surface corresponds to the requirement that finite tractions are needed to displace the interface. Thus, when this model is applied to study fracture, the cohesive zone tips are well defined. If (T_1, T_2) lies inside the initial yield surface, then interface displacement cannot occur and $\dot{\delta}_i = 0$. If (T_1, T_2) lies on the

initial yield surface $F(T_1, T_2) = C$, and if

$$-\dot{T}_i \partial F/\partial T_i > 0, \tag{53a}$$

then *unloading* is said to occur. For example, for initial yield surface of the form given by Eq. (52b), unloading occurs if

$$\dot{T}_i \partial F/\partial T_i = 2\dot{T}_1 T_1/\sigma_c^2 + 2\dot{T}_2 T_2/\tau_c^2 < 0. \tag{53b}$$

The case of $\dot{T}_i \partial F/\partial T_i = 0$ corresponds to continued motion of the interface without unloading, *i.e.*, the traction remains on the initial yield surface.

Since the interface can only soften as unloading occurs, subsequent unloading surfaces must have the form:

$$F(T_1, T_2, \phi) = 0. \tag{54a}$$

For example, if F is given by Eq. (52b), then

$$F(T_1, T_2, \phi) = (T_1/\sigma_c)^2 + (T_2/\tau_c)^2 = \phi^{-1}, \tag{54b}$$

where ϕ in Eq. (54b) is a state variable. Since $\phi = 1$ for the initial yield surface, and softening requires that subsequent yield surfaces shrink as interface deformation occurs, $\phi \geq 1$. The state variable ϕ can be interpreted as a damage parameter which causes softening of the interface.

As in plasticity, we propose the *normality rule*

$$\dot{\delta}_i = \dot{\lambda} \partial F/\partial T_i, \tag{55a}$$

where $\dot{\lambda}$ is a rate factor. This condition states that the incremental interfacial displacement is normal to the current yield surface. It is possible to derive Eq. (48) based on the normality rule, that is, rate-independent cohesive zone models can be generated based on the normality rule. The derivation is given in the Appendix.

For yield surfaces of the form given by Eq. (54b), the displacement rates using the normality condition Eq. (55a) are found to be:

$$\dot{\delta}_1 = 2\dot{\lambda} T_1/\sigma_c^2, \quad \dot{\delta}_2 = 2\dot{\lambda} T_2/\tau_c^2. \tag{55b}$$

Combining Eq. (55b) and the yield condition Eq. (54b), we have

$$\sigma_c^2 \dot{\delta}_1^2 + \tau_c^2 \dot{\delta}_2^2 = 4\dot{\lambda}^2 \phi^{-1}. \tag{56a}$$

Equation (56a) can be rewritten as

$$\dot{\lambda} = \frac{\sqrt{\sigma_c^2 \dot{\delta}_1^2 + \tau_c^2 \dot{\delta}_2^2}}{2} \sqrt{\phi} = \frac{\phi}{2}(T_1 \dot{\delta}_1 + T_2 \dot{\delta}_2). \tag{56b}$$

Thus, the rate factor is proportional to the power of interface dissipation. Combining Eqs. (55b) and (56b), the traction is

$$T_2 = \frac{\tau_c^2 \dot{\delta}_2}{2\dot{\lambda}} = \frac{\tau_c^2 \dot{\delta}_2}{\sqrt{\phi}\sqrt{\sigma_c^2 \dot{\delta}_1^2 + \tau_c^2 \dot{\delta}_2^2}} = \frac{\pm \tau_c}{\sqrt{\phi}\sqrt{(\sigma_c^2 \dot{\delta}_1^2 / \tau_c^2 \dot{\delta}_2^2) + 1}}, \tag{57a}$$

$$T_1 = \frac{\sigma_c^2 \dot{\delta}_1}{2\dot{\lambda}} = \frac{\sigma_c^2 \dot{\delta}_1}{\sqrt{\phi}\sqrt{\sigma_c^2 \dot{\delta}_1^2 + \tau_c^2 \dot{\delta}_2^2}} = \frac{\pm \sigma_c}{\sqrt{\phi}\sqrt{1 + (\tau_c^2 \dot{\delta}_2^2 / \sigma_c^2 \dot{\delta}_1^2)}}, \tag{57b}$$

which are special forms of Eq. (48). The shrinkage of the yield surface is measured by ϕ^{-1}. Because the interface softens as it unloads, we choose H to be a positive function so that ϕ is monotonically increasing. In a one-state variable model, the interface fails when the traction goes to zero, *i.e.*, when $\phi \to \infty$. Equations (50) and (57a,b) allow us to compute the traction history if the displacement history is given. We illustrate this by considering some special loading histories.

Pure Opening Mode

The simplest loading history is a purely opening mode where $\dot{\delta}_2 = 0$ and $\delta_1 = \Delta(t)$, where $\Delta(t)$ is a known function of t satisfying the condition $\Delta(t=0) = 0$. Here t denotes some monotonically increasing loading parameter. Since $\dot{\delta}_2 = 0$, $T_2 = 0$ by Eq. (57a). Equation (50) becomes

$$\dot{\phi} = |\dot{\delta}_1| H(\phi, 0) \equiv \dot{\delta}_1 H_I(\phi), \tag{58}$$

where we have assumed $\dot{\delta}_1 > 0$. Assuming that the initial state is on the initial yield surface, *i.e.*, $\phi = 1$ and $\delta_1 = 0$, the solution of Eq. (58) is

$$\int_1^{\phi} \frac{d\omega}{H_I(\omega)} = \int_0^t \dot{\delta}_1(\tau) d\tau \equiv \Delta(t). \tag{59}$$

As an example, we choose

$$H_I(\omega) = \omega / \delta_{cod}, \tag{60}$$

where δ_{cod} is a material constant. Substituting Eq. (60) into Eq. (59), we found

$$\phi = e^{\Delta(t)/\delta_{cod}}. \tag{61}$$

According to Eqs. (57b) and (61), T_1 is

$$T_1 = \frac{\sigma_c^2 \dot{\delta}_1}{2\dot{\lambda}} = \sigma_c / \sqrt{\phi} = \sigma_c e^{-\Delta(t)/2\delta_{cod}}. \tag{62}$$

For this particular loading history, the work to fail a unit area of the interface is

$$W_I = \int_0^\infty \sigma_1 d\Delta(t) = \sigma_c \int_0^\infty e^{-\Delta(t)/2\delta_{cod}} d\Delta = 2\sigma_c \delta_{cod}. \tag{63}$$

Proportional Loading

Consider the special case of *proportional loading* in displacement space, that is, consider loading histories of the form

$$\frac{\dot{\delta}_2}{\dot{\delta}_1} = \beta, \tag{64}$$

where β is a constant. As an example, consider a yield surface given by Eq. (56a). According to Eqs. (57a,b), proportional loading in the displacement space implies proportional loading in stress space, except that the proportional constant is different. Specifically,

$$\frac{\dot{\delta}_2}{\dot{\delta}_1} = \beta \Leftrightarrow \frac{T_2}{T_1} = \beta \left(\frac{\tau_c}{\sigma_c}\right)^2. \tag{65}$$

To simplify the mathematics, we assume $H\left(\phi, \tan^{-1}(\frac{\dot{\delta}_2}{\dot{\delta}_1})\right)$ is separable, that is,

$$H(\phi, \theta) = \frac{g(\theta)\phi}{\delta_{cod}}, \quad \left|\theta = \tan^{-1}(\dot{\delta}_2/\dot{\delta}_1) = \tan^{-1}\beta\right| \leq \pi/2. \tag{66}$$

Furthermore, we assume g is an even function. Note Eq. (66a) is consistent with Eq. (60) as long as

$$g(\theta = 0) = 1. \tag{67}$$

For proportional loading, Eq. (50) becomes

$$\dot{\phi} = \left|\dot{\delta}_1\right| \sqrt{1+\beta^2}\, g(\theta)\phi/\delta_{cod}, \tag{68}$$

where $\theta = \tan^{-1}\beta$. The solution of Eq. (68) is:

$$\phi = e^{\sqrt{1+\beta^2} g(\theta)\Delta(t)/\delta_{cod}}, \tag{69}$$

where $\Delta(t) = \int_0^t \dot{\delta}_1(\tau)d\tau$. The tractions can be computed using Eqs. (57a,b); they are:

$$T_2 = \frac{\tau_c}{\sqrt{(\sigma_c^2/\tau_c^2\beta^2)+1}} e^{-\sqrt{1+\beta^2}g(\theta)\Delta(t)/2\delta_{cod}}, \tag{70a}$$

$$T_1 = \frac{\pm\sigma_c}{\sqrt{1+(\tau_c^2\beta^2/\sigma_c^2)}} e^{-\sqrt{1+\beta^2}g(\theta)\Delta(t)/2\delta_{cod}}. \tag{70b}$$

Under proportional loading, the work to fail a unit area of the interface is

$$W = \int_o^\infty T_1 d\delta_1 + T_2 d\delta_2 = \int_o^\infty T_1 d\Delta + T_2|\beta| d\Delta$$
$$= \int_0^\infty \left[\frac{\sigma_c}{\sqrt{1+(\tau_c^2\beta^2/\sigma_c^2)}} + \frac{|\beta|\tau_c}{\sqrt{(\sigma_c^2/\tau_c^2\beta^2)+1}} \right] e^{-\sqrt{1+\beta^2}g(\theta)\Delta(t)/2\delta_{cod}} d\Delta. \tag{71a}$$

Evaluating the integral in Eq. (71a), we found

$$W = \frac{2\sigma_c\delta_{cod}}{\sqrt{1+\beta^2}g(\theta)} \left[\frac{1}{\sqrt{1+(\tau_c^2\beta^2/\sigma_c^2)}} + \frac{|\beta|\tau_c/\sigma_c}{\sqrt{(\sigma_c^2/\tau_c^2\beta^2)+1}} \right]. \tag{71b}$$

By definition, $\beta \to \pm\infty$ corresponds to pure Mode II deformation where $\delta_1 = 0$ and $\delta_2 \equiv \Lambda(t)$. In this limit, $\sqrt{1+\beta^2}\Delta \to \Lambda$, and Eq. (71b) reduces to

$$W \to W_{II} = \frac{2\tau_c\delta_{cod}}{g(\pi/2)}. \tag{72a}$$

According to Eqs. (63) and (72a), the condition for $W_{II} > W_I$ is

$$g(\pi/2) < \tau_c/\sigma_c. \tag{72b}$$

Clearly, there are infinitely many even functions, g, that satisfy Eqs. (67) and (72b). A reasonable choice is to choose g with the following properties: g achieves its absolute maximum at $\theta = 0$, monotonically increasing for $\theta < 0$ and monotonically decreasing for $\theta > 0$ (*e.g.*, $g(\theta) = 1 - \frac{4(1-\omega)}{\pi^2}\theta^2$, $0 < \omega < \tau_c/\sigma_c$). It is interesting to note that a potential function Φ does not exist (*i.e.*, $T_i = \partial\Phi/\partial\delta_i$) even if the loading history is confined to proportional loading. Indeed, it is easy to verify that

[using Eqs. (70a,b)]:

$$\frac{\partial T_1}{\partial \delta_2} = \frac{\partial T_1}{\beta \partial \Delta} \neq \frac{\partial T_2}{\partial \delta_1} = \frac{\partial T_2}{\partial \Delta}. \tag{73}$$

Using Eq. (72a), Eq. (71) can be rewritten as

$$W = \frac{W_I}{\sqrt{1+\beta^2 g(\theta)}} \sqrt{1 + [\beta g(\pi/2)]^2 \left(\frac{W_{II}}{W_I}\right)^2}. \tag{74}$$

It is easy to see that $W_I \leq W \leq W_{II}$.

Loading in Mode I and followed by Mode II

Consider the evolution of the interface traction when a pure opening displacement $\Delta(t)$ is applied during $0 < t < t_o$, followed by the application of a sliding displacement. Specifically, we impose the following displacement history:

$$\dot{\delta}_1 > 0 \Rightarrow \delta_1 = \int_o^t \dot{\delta}_1(\tau) d\tau \equiv \Delta(t),\ \dot{\delta}_2 = 0 \quad 0 < t < t_o, \tag{75a}$$

$$\dot{\delta}_1 = 0, \dot{\delta}_2 > 0, \Lambda(t) \equiv \int_{t_o}^t \dot{\delta}_2(\tau) d\tau \quad t > t_o, \tag{75b}$$

where Δ, Λ are monotonic increasing functions of t that satisfy the conditions

$$\Delta(0) = \Lambda(t_o) = 0. \tag{76}$$

The interface traction for $0 < t < t_o$ is given by Eq. (63), *i.e.*,

$$T_1 = \sigma_c e^{-\Delta(t)/2\delta_{cod}}, \quad T_2 = 0. \quad 0 < t < t_o. \tag{77}$$

For $t > t_o$, $T_1 = 0$ by Eq. (57b) and $T_2 = \tau_c/\sqrt{\phi}$ by Eq. (57a). The damage, ϕ, is determined by solving Eq. (50) with H given by Eq. (66) and the initial condition $\phi(t_o) = e^{\Delta(t_o)/\delta_{cod}}$, as required by Eq. (61). The solution is

$$\phi = e^{\Delta(t_o)/\delta_{cod}} e^{g(\pi/2)\Lambda(t)/\delta_{cod}}. \tag{78a}$$

Using Eqs. (57a,b), the traction is

$$T_2 = \tau_c e^{-\Delta(t_o)/2\delta_{cod}} e^{-g(\pi/2)\Lambda(t)/2\delta_{cod}}, \quad T_1 = 0, \quad t > t_o. \tag{78b}$$

The work to fail a unit area of the interface or adhesion energy is found to be

$$2\sigma_c\delta_{cod}(1-e^{-\Delta(t_o)/2\delta_{cod}})+\frac{2\tau_c\delta_{cod}}{g(\pi/2)}e^{-\Delta(t_o)/2\delta_{cod}}=W_I+(W_{II}-W_I)e^{-\Delta(t_o)/2\delta_{cod}}, \tag{79}$$

where $W_{II}=\frac{2\tau_c\delta_{cod}}{g(\pi/2)}$. It is interesting to compare this adhesion energy with the adhesion energy if the interface were to fail by proportional loading, which is given by Eq. (74). Note that the traction is discontinuous at $t=t_o$.

Loading and Unloading in Mode II

Consider the following loading history where $\delta_1=0$ for all times. The normality rule states that $T_1=0$. The stress state initially is on the yield surface given by Eq. (56a), *i.e.*, $T_1=0$, $T_2=\tau_c$. The evolution of state is governed by Eq. (50) with H by Eq. (66). The traction is

$$T_1=0,\quad T_2=\frac{\pm\tau_c}{\sqrt{\phi}}. \tag{80}$$

As before, we assume that g is an even function of θ. Let $\delta_2(t)=\Lambda(t)$ for $t_1>t\geq 0$, where $\Lambda(t)$is a positive continuous function for $t>0$. In addition, $\Lambda(t=0)=0$. Equation (50) implies that

$$\dot{\phi}=|\dot{\delta}_2|H(\phi,\theta)=|\dot{\delta}_2|\frac{g(\pi/2)\phi}{\delta_{cod}}. \tag{81a}$$

The argument of g is $\pi/2$ since g is even. Integrating Eq. (81), for $t_1>t\geq 0$,

$$\phi=e^{\Lambda(t)\frac{g(\pi/2)}{\delta_{cod}}}. \tag{81b}$$

The shear traction is

$$T_2=\tau_c e^{-g(\pi/2)\Lambda(t)/2\delta_{cod}}. \tag{82}$$

Suppose at $t=t_1$, the loading rate is suddenly reversed to $\dot{\delta}_2=-\dot{\Lambda}(t_1)$. According to Eq. (50), this sudden reversal does not change the state variable. However, Eq. (57b) implies that the traction is discontinuous at $t=t_1$. Specifically, the traction reverses sign, *i.e.*, $T_2(t_1^+)=\frac{-\tau_c}{\sqrt{\phi(t_1)}}=-T_2(t_1^-)$. For $t>t_1$, the traction is given by

$$T_2=-\tau_c e^{-\Lambda(t)g(\pi/2)/2\delta_{cod}}\qquad t>t_1. \tag{83}$$

It is clear that this process of displacement rate reversal can be carried out indefinitely. The traction reverses sign each time the displacement

rate is reversed. However, the work needed to fail a unit area of the interface is still W_{II}, irrespective of the number of loading rate reversals.

4.3. Interface Model with Initial Hardening

The above theory can also be used to describe interfaces that exhibit initial hardening. For example, consider yield functions of the form:

$$F(T_1, T_2, \phi) = (T_1/\sigma_c)^2 + (T_2/\tau_c)^2 = \rho(\phi), \tag{84}$$

where ρ is a smooth function of the state variable ϕ. The function ρ is assumed to have the following behavior:

$$d\rho/d\phi > 0 \quad \phi_o \le \phi < \phi^* \qquad \text{(hardening branch)}, \tag{85a}$$

$$d\rho/d\phi < 0 \quad \phi > \phi^* \qquad \text{(softening branch)}, \tag{85b}$$

$$\rho(\phi \to \infty) = 0 \qquad \text{(interface fail, yield surface collapse)}, \tag{85c}$$

$$\rho(\phi_o) = 0 \tag{85d}$$

where ϕ_o denotes the state of a undamaged interface with no deformation. Since $\rho(\phi_o) = 0$, the cohesive zone front does not exist.

Using Eq. (55a) we again get Eq. (55b); combining with the yield condition Eq. (84), $\dot{\lambda}$ is found to be

$$\dot{\lambda} = \frac{\sqrt{\sigma_c^2 \dot{\delta}_1^2 + \tau_c^2 \dot{\delta}_2^2}}{2\sqrt{\rho(\phi)}} \tag{86}$$

and

$$\dot{\phi} = \sqrt{\dot{\delta}_1^2 + \dot{\delta}_2^2} H(\phi, \theta) = \sqrt{\dot{\delta}_1^2 + \dot{\delta}_2^2} \frac{g(\theta)\phi}{\delta_{cod}}, \tag{87}$$

with $g(0) = 1$. As an example, consider

$$\rho(\phi) = \frac{\phi - 1}{\phi^2}, \tag{88}$$

where $\phi \ge \phi_o = 1$. If the interface fails under Mode I condition, then

$$T_1 = \sigma_c \frac{\sqrt{\phi - 1}}{\phi}, \tag{89a}$$

where

$$\phi = e^{\Delta(t)/\delta_{cod}}. \tag{89b}$$

The work to fail a unit area of the interface in tension is

$$W_I = \int_0^\infty T_1 d\Delta = \sigma_c \delta_{cod} \int_0^\infty e^{-\eta}\sqrt{e^\eta - 1}\, d\eta = \frac{\pi}{2}\sigma_c \delta_{cod}. \tag{90}$$

The solution for proportional loading can also be found. The state variable evolves in the same way, *i.e.*,

$$\phi = e^{\sqrt{1+\beta^2} g(\theta)\Delta(t)/\delta_{cod}}. \tag{91}$$

The traction T_1 is found to be

$$T_1 = \frac{\sigma_c}{\sqrt{1 + (\tau_c^2\beta^2/\sigma_c^2)}}\sqrt{\rho(\phi)} = \frac{\sigma_c}{\sqrt{1 + (\tau_c^2\beta^2/\sigma_c^2)}}\frac{\sqrt{\phi - 1}}{\phi}, \tag{92}$$

where ϕ is given by Eq. (91) and T_2 can be found from Eq. (65). The work to fail an interface under proportional loading is:

$$\begin{aligned} W &= \int_o^\infty T_1 d\delta_1 + T_2 d\delta_2 = (1 + \frac{\beta^2\tau_c^2}{\sigma_c^2}) \int_o^\infty T_1 d\Delta \\ &= \sigma_c \sqrt{1 + (\tau_c^2\beta^2/\sigma_c^2)} \int_0^\infty \sqrt{\rho(\phi)} d\phi = W_I \sqrt{1 + (\tau_c^2\beta^2/\sigma_c^2)}. \end{aligned} \tag{93}$$

4.4. Work and Loading History

The work to fail or to deform an interface is history-dependent. This can be seen by computing the work need to deform a unit area of the interface from $\delta_1 = \delta_2 = 0$ to $\delta_1 = \Delta_1$ and $\delta_2 = \Lambda_2 = \beta\Delta_1$ using two loading histories. In the first loading path we start by opening the interface, then apply a slip displacement [see Eqs. (75a,b)]. The work done along this path is:

$$\begin{aligned} &2\sigma_c\delta_{cod}(1 - e^{-\Delta_1/2\delta_{cod}}) + \frac{2\tau_c\delta_{cod}}{g(\pi/2)} e^{-\Delta_1/2\delta_{cod}}(1 - e^{-\Lambda_2/2\delta_{cod}}) \\ &\quad = W_I + (W_{II} - W_I)e^{-\Delta_1/2\delta_{cod}} - W_{II}e^{-(1+|\beta|)\Delta_1/2\delta_{cod}}. \end{aligned} \tag{94}$$

On the other hand, if the loading is proportional, then the work done on a unit interfacial area from (0, 0) to (Δ_1, Λ_2) is

$$W = \int_o^{\Delta_1} T_1 d\delta_1 + \int_o^{\Lambda_2} T_2 d\delta_2 = (1 + \frac{\beta^2 \tau_c^2}{\sigma_c^2}) \int_o^{\Delta_1} T_1 d\delta_1$$
$$= \frac{W_I \sqrt{1 + (\tau_c^2 \beta^2 / \sigma_c^2)}}{\sqrt{1 + \beta^2} g(\theta)} \left(1 - e^{-\frac{\sqrt{1+\beta^2} g(\theta) \Delta_1}{2\delta_{cod}}}\right). \tag{95}$$

Thus, the energy dissipated is path dependent.

5. STABILITY OF COHESIVE ZONE INTERFACES

5.1. Stability of Interface in Homogeneous Deformation

Cohesive zone models are commonly used to model growth of *preexisting* cracks. A much more difficult problem is how these cracks nucleate. Since an important aspect of cohesive zone models is the softening of interface, it is natural to study the stability of the deformation of a continuum interface point. In Section 5.2, we show that interfacial instability leads to crack nucleation (See [80] for a related treatment.). We start by considering the stability of an interface undergoing a spatially homogeneous deformation. Let us assume that the motion of the interface is described by a form of Eqs. (46a,b) where the f_i and h are explicitly independent of rates, *i.e.*,

$$T_i = f_i(\delta_1, \delta_2, \delta_3, \phi), \tag{96a}$$
$$\dot{\phi} = h(\delta_1, \delta_2, \delta_3, \phi)). \tag{96b}$$

Consider the special case $\delta_2 = \delta_3 = 0$. Also, assume $T_2 = T_3 = 0$. For this case, we have:

$$T = f(\delta, \phi), \tag{97a}$$
$$\dot{\phi} = h(\delta, \phi), \tag{97b}$$

where $T \equiv T_1, f \equiv f_1, \delta \equiv \delta_1$. In general, there are many non-trivial spatially homogeneous steady state solutions where $\delta = \delta_0$ and $\phi = \phi_0$ where δ_0, ϕ_0 are constants. We are interested in the stability of these steady states.

Figure 10 shows the schematics of the loading device which is represented by the spring. Here we regard the cohesive zone as a mechanical system and the structure surrounding it as the loading device. For example, the loading device can be a load cell in series with the material outside the interface. Since the stiffness of the material

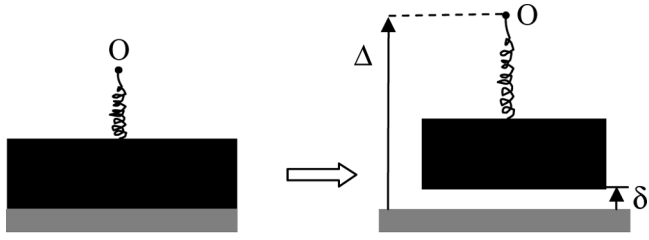

FIGURE 10 (a) A flat interface (not shown) sandwiched between a infinite rigid block and an infinite rigid substrate; no load is applied to the block. (b) A fixed vertical displacement is applied to O. The spring represents the stiffness of the loading device and $\delta > 0$ is the spatially homogeneous interfacial displacement.

outside the cohesive interface is represented by the spring, we envision the interface sandwiched between an infinite rigid block and an infinite rigid substrate.

The equation of motion of the block is:

$$m\ddot{\delta} = k(\Delta - \delta) - f(\delta, \phi), \tag{98}$$

where m is the mass of the block per unit contact area, k is the stiffness of the loading device (units of k = force per unit volume), f is the normal stress acting on the block, and Δ is the fixed applied displacement. To study stability of the steady state(δ_o, ϕ_o), let

$$\delta = \delta_o + \varepsilon_1(t), \tag{99a}$$
$$\phi = \phi_o + \varepsilon_2(t), \tag{99b}$$

where $|\varepsilon_i| << 1$. Substituting Eqs. (99a,b) into Eq. (98) and Eq. (97b) and expanding about the steady state (δ_o, ϕ_o) gives:

$$m\ddot{\varepsilon}_1 = [k(\Delta - \delta_0) - f(\delta_0, \phi_0)] - k\varepsilon_1 - f_1\varepsilon_1 - f_2\varepsilon_2, \tag{100a}$$
$$\dot{\varepsilon}_2 = [h(\delta_0, \phi_0)] + h_1\varepsilon_1 + h_2\varepsilon_2, . \tag{100b}$$

where $f_1 \equiv \frac{\partial f}{\partial \delta}\Big|_{\delta_0,\phi_0}, f_2 \equiv \frac{\partial f}{\partial \phi}\Big|_{\delta_0,\phi_0}, h_1 \equiv \frac{\partial h}{\partial \delta}\Big|_{\delta_0,\phi_0}, h_2 \equiv \frac{\partial h}{\partial \phi}\Big|_{\delta_0,\phi_0}$. The terms in the square brackets in Eqs. (100a,b) are identically zero by assumption, so

$$m\ddot{\varepsilon}_1 = -k\varepsilon_1 - f_1\varepsilon_1 - f_2\varepsilon_2, \tag{101a}$$
$$\dot{\varepsilon}_2 = h_1\varepsilon_1 + h_2\varepsilon_2. \tag{101b}$$

The stability of the linear system of ordinary differential Eqs. (101a,b) can be readily worked out using the Laplace transform. It depends on the roots of the algebraic equation

$$(s - h_2)(ms^2 + k + f_1) - f_2 h_1 = 0. \tag{102}$$

The solution of Eqs. (101a,b) is unstable (grows exponentially with time) if any of the roots of Eq. (102) have positive real parts.

As an example, consider the special case where a potential exists. For this case, the stability criterion can be obtained formally by setting $h = 0$ and f independent of ϕ in Eqs. (97a,b). Let f have the shape shown in Fig. 11 for $\delta > 0$.

The stability condition Eq. (102), for this case, reduces to

$$s = \pm\sqrt{-(k + f'(\delta_o))/m}. \tag{103}$$

Note that if $\delta_0 = \delta_0^- < \delta^*$, then the spatially homogeneous solution $T = \sigma_0, \delta = \delta_0^-$ is neutrally stable since $k + f'(\delta_0^-) > 0$, where $f' \equiv df/d\delta$. On the other hand, if

$$k + f'(\delta_0^+) < 0, \tag{104}$$

one of the roots has a positive real part, so the spatially homogeneous solution $T = \sigma_0, \delta = \delta_0^+$ is unstable. The instability condition Eq. (104) can be written as

$$k < k_c, \tag{105}$$

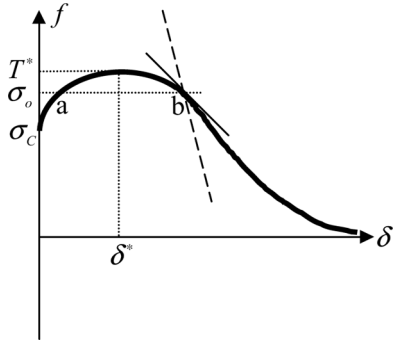

FIGURE 11 A special case of $T = f(\delta)$. The potential function is $\Phi(\delta) = \int_0^\delta f(\delta')d\delta'$. Note, for any $0 < \sigma_1 \leq T^*$, there are two equilibrium interfacial displacements $\delta_o = \delta_0^\pm$ (corresponding to points a (δ_0^-), b (δ_0^+) in Fig. 11). The line tangent to the curve at b has slope $f'(\delta_0^+)$. The stiffness of the loading device is the dashed line with slope $-k$.

where $k_c \equiv -f'(\delta_0^+)$ is the critical stiffness. Note that k_c is an intrinsic property of the interface. Equation (104) has the following physical interpretation: homogeneous deformation of the interface is stable if the loading device is always stiffer than the intrinsic stiffness of the interface (as defined by the tangent lines in Fig. 11); otherwise, the interface is unstable for some value of its opening.

A different way to obtain Eq. (105) without using inertia and taking the formal limit of $h \to 0$ is to introduce some small rate dependence in the potential model, *e.g.*, assume

$$T = f(\delta) + \beta\dot{\delta}, \tag{106}$$

where $\beta > 0$ is a small damping term. Perturbing about the equilibrium state $T = \sigma_0$, $\delta = \delta_0^+$ gives:

$$\left[k + f'(\delta_0^+)\right]\varepsilon_1 + \beta\dot{\varepsilon}_1 = 0. \tag{107}$$

As before, the perturbation grows exponentially if $k + f'(\delta_0^+) < 0$ or $k < -f'(\delta_0^+) \equiv k_c$.

5.2. Stability of Continuous Systems: Crack Nucleation and Growth

The above analysis suggests that an interface subjected to homogeneous deformation can nucleate cracks and these cracks can evolve. To study this phenomenon, it is necessary to include the elasticity of the material outside the interface. For simplicity, we restrict our analysis to potential interface models and assume $T_2 = T_3 = \delta_2 = \delta_3 = 0$. Figure 12 shows the geometry. Let the interface be the xz plane and the infinitely extended, homogeneous bulk material on both sides of it be linearly elastic with shear modulus, G, and Poisson's ratio, v, respectively. We assume plane strain deformation.

We assume the interface model has the form:

$$F(T, \delta) = 0 \quad \delta \geq 0, \tag{108}$$

where $T = \sigma_{22}(x, y = 0)$ and $\delta = v(x, y = 0^+) - v(x, y = 0^-)$. For $\delta > 0$, we assume that Eq. (108) can be solved to give

$$T = f(\delta). \tag{109}$$

The function f is sketched in Fig. 11. The boundary conditions at infinity are:

$$\sigma_{22}(x, |y| \to \infty) = \sigma_0, \sigma_{21}(x, |y| \to \infty) = 0. \tag{110}$$

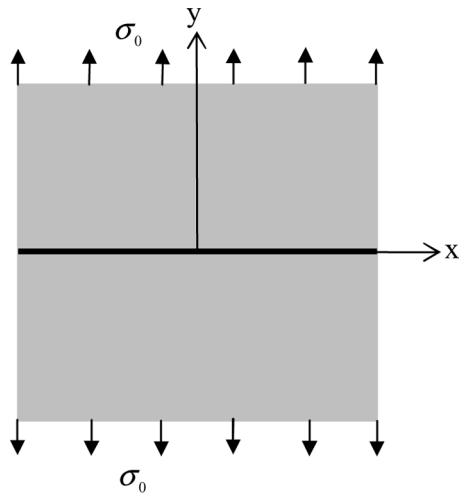

FIGURE 12 A cross-section of an infinite block of linear elastic solid subjected to remote tension. The interface occupies the *xz* plane.

The boundary conditions on the interface are:

$$\sigma_{21}(x, y = 0) = 0, \tag{111}$$

$$T = f(\delta). \tag{112}$$

For $\sigma_o > \sigma_C$, where σ_C is the cohesive stress (see Fig. 11), there exists a homogenous equilibrium solution which gives *non-zero* interface displacement, δ_0^+. The horizontal and vertical displacements associated with these homogeneous solutions are

$$u_0(x,y) = \frac{-\nu\sigma_0}{2G}x, \quad v_0(x,y) = \begin{cases} \frac{(1-\nu)\sigma_0}{2G}y + \delta_0^+ & y > 0 \\ \frac{(1-\nu)\sigma_0}{2G}y & y < 0 \end{cases}, \tag{113a}$$

respectively. The stresses associated with these displacements are spatially homogeneous. They are:

$$\sigma_{22}^0(x,y) = \sigma_o, \sigma_{12}^0(x,y) = \sigma_{11}^0(x,y) = 0. \tag{113b}$$

The normal traction on the interface is $\sigma_o \equiv T_o$ and is related to the interface displacement δ_0^+ by Eq. (112), *i.e.*,

$$T_o = f(\delta_0^+). \tag{113c}$$

We now show that this homogenous equilibrium state is in general unstable to spatial perturbations and will evolve into one of the

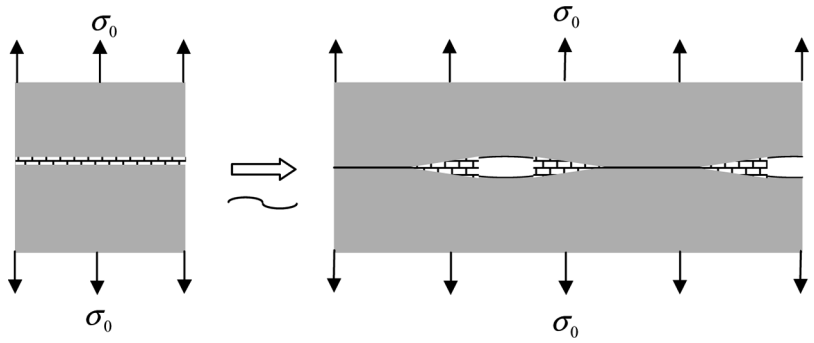

FIGURE 13 (a) Interface under homogeneous deformation. (b) After perturbation, the homogenous state in (a) evolves into an interface with traction free cracks, cohesive zone, and intact zones.

infinitely many possible equilibrium states illustrated in Fig. 13. These bifurcated equilibrium states are possible because the interface model allows solutions in the form of traction-free cracks and cohesive zones that can support normal stresses on the interface.

To study stability of the homogenous equilibrium state given by Eqs. (113a–c) and to find the conditions under which these instabilities occur, we impose a small sinusoidal perturbation of the form

$$\delta(x,t) = \delta_0^+ + \varepsilon(t)\sin\kappa x \quad \kappa = 2\pi/\lambda > 0 \quad \varepsilon << 1, \tag{114a}$$

on the interface, where t denotes time and λ is the wavelength of the perturbation. To capture stability, we modify our interface model to Eq. (106). The displacement fields can be written as

$$v = v_o + v_p, \tag{114b}$$

$$u = u_o + u_p, \tag{114c}$$

where v_p and u_p are the perturbed fields. Also, let σ_{ij}^p denote the stresses associated with the perturbed field. Note that any reasonable spatial perturbation can be represented by a Fourier sine series so our approach is quite general. Finally, the symmetry of the problem allows us to restrict our attention to the upper half plane, $y > 0$. Note that

$$\begin{aligned} &\sigma_{22}(x, y=0, t) = f\left((\delta_0^+ + \varepsilon(t)\sin kx)\right) + \beta\dot{\delta}(x,t) \Rightarrow \\ &\sigma_{22}^0(x, y=0, t) + \sigma_{22}^p(x, y=0, t) = \\ &= f(\delta_0^+) + f_1\varepsilon(t)\sin kx + \beta\dot{\varepsilon}(t)\sin kx, \end{aligned} \tag{115}$$

where $f_1 \equiv f'(\delta_0^+)$. By Eq. (113c), we have $\sigma_{22}^0(x, y=0) = T_o = f(\delta_0^+)$, so

$$T_p \equiv \sigma_{22}^p(x, y=0, t) = f_1 \varepsilon(t) \sin kx + \beta \dot{\varepsilon}(t) \sin kx. \tag{116a}$$

The other boundary conditions are

$$\sigma_{22}^p(x, y=\infty, t) = \sigma_{21}^p(x, y=\infty, t) = 0, \tag{116b}$$
$$\sigma_{12}^p(x, y=0, t) = 0. \tag{116c}$$

It can be easily shown that the stress function

$$\chi = c(t) e^{-\kappa y}[1 + \kappa y] \sin \kappa x, \tag{117}$$

satisfies the boundary conditions Eqs. (116b,c). According to Eq. (117), the normal traction on the interface $y = 0$ is

$$T_p = -\kappa^2 c(t) \sin \kappa x. \tag{118}$$

Substituting Eq. (118) into Eq. (116a), we obtain

$$-k^2 c(t) = f_1 \varepsilon(t) + \beta \dot{\varepsilon}(t). \tag{119}$$

The vertical perturbed elastic displacement can be found using Eq. (117). It is

$$v_p(x, y, t) = \frac{[2(1-\nu) + \kappa y]}{2G} \kappa e^{-\kappa y} c(t) \sin \kappa x. \tag{120}$$

At $y = 0^+$, $v_p(x, y = 0^+, t) = \delta_p = \varepsilon(t) \sin \kappa x$. This fact, together with Eq. (120), gives

$$\varepsilon(t) = \frac{(1-\nu)}{G} \kappa c(t). \tag{121}$$

Substituting Eq. (121) into Eq. (119), we have

$$\left[f_1 + \frac{G\kappa}{(1-\nu)} \right] c(t) + \beta \dot{c}(t) = 0. \tag{122}$$

Equation (122) implies that c grows exponentially fast if

$$\frac{G\kappa}{(1-\nu)} < -f_1 = -f'(\delta_0^+). \tag{123}$$

Recall $-f'(\delta_0^+) > 0$ (see Fig. 11). Equation (123) implies that the homogeneous solution is unstable if

$$\lambda > \lambda_c \equiv \frac{2\pi}{(1-\nu)} \frac{G}{\left|f'(\delta_0^+)\right|}. \tag{124}$$

Thus, all wavelengths above $\lambda_c$are unstable. Since perturbations in general contain all wavelengths (*e.g.*, white noise), interfaces that soften are invariably unstable.

6. SUMMARY AND DISCUSSIONS

The cohesive zone approach to modeling the mechanics of fracture, while introduced early in the development of the subject, has been used much more widely over the last 15 years. From the perspective of physical modeling, it provides a natural link between micromechanics and continuum scale modeling. It is also convenient for computational modeling of fracture since cohesive zone models are readily implemented as cohesive elements in finite element analysis.

Despite their widespread use, insufficient attention has been paid to examine systematically different classes of cohesive zone models from the view point of their representation of interfacial constitutive behavior, and this has been the topic of this paper. In particular, with only a few references to specific material models, we lay out different classes of cohesive interfacial models, to a significant extent in analogy with models for bulk elastic and inelastic behavior of materials. The basic kinematic quantity is the interfacial opening displacement vector, which is defined as the difference of separation between remote points on either side of the interface and the value of separation between equivalent points in a material with the same bulk properties but without the damaging interface. The cohesive zone model relates these kinematic quantities and its rates of change to the traction acting on the interface. We show that if the interface can support some traction without opening, then a cohesive zone tip can exist. Similarly, existence of a crack-tip is contingent on there being a finite opening at which tractions reduce to zero.

One class of cohesive zone models is such that tractions can be derived as gradients of a potential, defined as a function of opening

displacements. We consider a few examples and show that models with an initial hardening branch of the traction-displacement relation can generally suffer from unphysical material softening and interpenetration. Often, potential-based cohesive zone models have a phase-angle-independent work of opening the interface. We show that while it is possible to construct potentials with directionally dependent fracture energy, such models violate steady state crack growth under small-scale yielding conditions. Instead, we show that anisotropy can be built in by working with a conventional potential and adding a direction-dependent condition that cuts it off at a critical crack opening displacement. We examine conditions under which multiple crack and cohesive fronts can exist.

Our discussion of general rate-dependent cohesive zone models is very cursory, but we do examine rate-independent history-dependent models in some detail. Specifically, we develop them in analogy with classical plasticity by defining a yield surface in the space of interfacial tractions, which is used to derive opening displacements. These are examined in a few simple cases of loading paths.

In the last section of this work we consider the stability of cohesive zone interfaces. Our example is based on an earlier work [20] and is restricted to interfaces in homogeneous linear elastic solids and for a simple class of cohesive zone models. However, many of the basic ideas can be extended to bimaterial systems and to more complicated cohesive zone models.

ACKNOWLEDGMENT

C. Y. Hui enjoyed the many discussions with S. Vavasis and K. Papoulia of University of Waterloo while both of them were at Cornell. Rong Long acknowledges the support from Materials and Surface Engineering program, CMMI, National Science Foundation (Grant no: CMMI-0900586). C. Y. Hui and A. Jagota acknowledge the support from the Department of Energy, Office of Basic Science, Division of Material Science and Engineering (Grant no: DE-FG02-07ER46463).

REFERENCES

[1] Barenblatt, G. I., *Advances in Applied Mechanics* **7**, 56–129 (1962).
[2] Cottrell, A. H., Mechanics of fracture, in *Tewksbury Symposium of Fracture*, C. J. Osborn, ed. (University of Melbourne, Australia, 1963), pp. 1–27.
[3] Bilby, B. A., Cottrell, A. H., and Swinden, K. H., *Proc. Roy. Soc. London, Ser A* **272**, 304–314 (1963).

[4] Knauss, W. G., On the steady propagation of a crack in a viscoelastic sheet: Experiments and analysis, in *Deformation and Fracture of High Polymers*, H. H. Kausch, J. A. Hassell and R. I. Jaffee (Eds.) (Plenum Press, New York, 1974), pp. 501–541.
[5] Schapery, R. A., *Int. J. Fracture* **11**, 141–159 (1975).
[6] Hui, C. Y., Xu, D. B., and Kramer, E. J., *J. Appl. Phys.* **72**, 3294–3304 (1992).
[7] Xu, D. B., Hui, C. Y., and Kramer, E. J., *J. Appl. Phys.* **72**, 3305–3316 (1992).
[8] Maugis, D., *Colloid Interface Sci.* **150**, 243–267 (1992).
[9] Lin, Y. Y. and Hui, C. Y., *J. Polym. Sci.: Part B: Polymer Physics* **40**, 772–793 (2002).
[10] Johnson, K. L., in *Microstructure and Microtribology of Polymer Surfaces*, V. V. Tsukruk and K. J. Wahl (Eds.) (American Chemical Society, Washington, DC, 2000), p. 24.
[11] Barthel, E. and Haiat, G., *Langmuir* **18**, 9362–9370 (2002).
[12] Ruina, A. L., *J. Geophys. Res.* **88**, 10359–10370 (1983).
[13] Ruina, A. L., Constitutive relations for frictional slip, in *Mechanics of Geomaterials*, Z. P. Bazant (Ed.) (John Wiley, New York, 1984), pp. 169–187.
[14] Dieterich, J. H., Constitutive properties of faults with simulated gouge, in Mechanical behavior of Crustal Rocks, in *Geophys. Monogr. Ser.*, N. L. Carter, M. Friedman, J. M. Logan and D. W. Stearns (Eds.) (AGU, Washington, DC, 1981), Vol. 24, pp. 103–120.
[15] Lin, Y. Y., Hui, C. Y., and Jagota, A., *Colloid Interface Sci.* **237**, 267–282 (2001).
[16] Hui, C. Y., Ruina, A., Creton, C., and Kramer, E. J., *Macromolecules* **25**, 3948–3955 (1992).
[17] Sha, Y., Hui, C. Y., Ruina, A. L., and Kramer, E. J., *Acta Mater.* **45**, 3555–3563 (1997).
[18] Wang, W.-C. V. and Kramer, E. J., *J. Material Science* **17**, 2013–2026 (1982).
[19] Ungsuwarungsri, T. and Knauss, W. G., *J. Applied Mechanics* **110**, 44–51 (1988).
[20] Hui, C. Y., Lagoudas, D., and Ruina, A. L., Constitutive models for crazes and their effects on crack growth in glassy polymers, in *Constitutive Modeling for Non-Traditional Materials*, V. K. Stokes and D. Krajcinovic (Eds.) (ASME, New York, 1987), pp. 85–115.
[21] Rahul-Kumar, P., Jagota, A., Bennison, S. J., and Saigal, S., *Intl. J. Solids and Structures* **37**, 1873–1897 (2000).
[22] Jagota, A., Bennison, S. J., and Smith, C. A., *Intl. J. Fracture* **104**, 105–130 (2000).
[23] Ghatak, A., Vorvolakos, K., She, H., Malotky, D., and Chaudhury, M. K., *J. Phys. Chem. B* **104**, 4018–4030 (2000).
[24] Bao, G. and Suo, Z., *Appl. Mech. Rev.* **24**, 355–366 (1992).
[25] Hutchinson, J. W. and Jenson, H. M., *Mech. Mater.* **9**, 139–163 (1990).
[26] Marshall, D. B., Cox, B. N., and Evan, A. G., *Acta Metall.* **35**, 2607–2619 (1985).
[27] Rose, L. R. F., *J. Mech. Phys. Solids* **35**, 383–405 (1987).
[28] McCartney, L. N., *Proc. R. Soc. Lond. A.* **409**, 329–350 (1987).
[29] Needleman, A., *J. Applied Mechanics* **54**, 525–531 (1987).
[30] Needleman, A., *J. Mech. Phys. Solids* **38**, 289–324 (1990).
[31] Suo, Z., Ortiz, M., and Needleman, A., *J. Mech. Phys. Solids* **40**, 613–640 (1992).
[32] Kogan, L., Hui, C. Y., and Ruina, A. L., *Macromolecules* **29**, Part I, 4090–4100; Part II 4101–4106 (1996).
[33] Horowitz, F. G. and Ruina, A., *J. Geophysical Research* **94**, 10279–10298 (1989).
[34] Rice, J. R. and Ruina, A., *J. Applied Mechanics* **50**, 343–349 (1983).
[35] Ortiz, M., Leroy Y., and Needleman, A., *Computer Methods in Applied Mechanics and Engineering* **61**, 189–214 (1987).
[36] Tvergaard, V. and Hutchinson, J. W., *J. Mech. Phys. Solids* **40**, 1377–1397 (1992).

[37] Tvergaard, V. and Hutchinson, J. W., *J. Mech. Phys. Solids* **41**, 1119–1135 (1993).
[38] Belytchko, T., Fish, J., and Englemann, B. E., *Computer Methods in Applied Mehanics and Engineering* **70**, 59–89 (1988).
[39] Olofsson, T. H., Klisinski, M., and Nedar, P., Inner softening bands: a new approach to localization in finite elements, in *Computation Modeling of Concrete Structures*, H. Mang, N. Bicanic and R. de Borst (Eds.) (Pineridge Press, Swansea, 1994), pp. 373–382.
[40] Xu, X-P. and Needleman, A., *J. Mech. Phys. Solids* **42**, 1397–1434 (1994).
[41] Chaboche, J. L., Girard, R., and Levasseur, P., *Int. J. Damage Mechanics* **6**, 220–257 (1997).
[42] Jirasek, M. and Zimmermann, T., *Intl. J. Numer. Meth. Engng* **50**, 1269–1290 (2001).
[43] Rahul-Kumar, P., Jagota, A., Bennison, S. J., Saigal, S., and Muralidhar, S., *Acta Materialia* **47**, 4161–4169 (1999).
[44] Camacho, G. T. and Ortiz, M., *Intl. J. Solids and Structures* **33**, 2899–2938 (1996).
[45] Pandolfi, A., Krysl, P., and Ortiz, M., *Intl. J. Fracture* **95**, 279–297 (1999).
[46] Needleman, A., *Computational Mechanics* **19**, 463–469 (1997).
[47] Falk, M. L., Needleman, A., and Rice, J. R., *Jounal de Physique IV* **11**, pr5-43-pr5-50 (2001).
[48] Ortiz, M. and Pandolfi, A., *Int. J. Numer. Meth. Engng.* **44**, 1269–1282 (1999).
[49] Ortiz, M. and Suresh, S., *J. Applied Mechanics* **60**, 77–84 (1993).
[50] Zhang, X., Mai, Y. W., and Jeffrey, R. G., *Int. J. Solids and Structures* **40**, 5819–5837 (2003).
[51] Yang, Q. D., Thouless, M. D., and Ward, S. M., *J. Adhesion* **72**, 115–132 (2000).
[52] Yang, Q. D., Thouless, M. D., and Ward, S. M., *Intl. J. Solids Structure* **38**, 3251–3262 (2001).
[53] Andena, L., Rink, M. and Williams, J. G., *Engineering Fracture Mechanics* **73**, 2476–2485 (2006).
[54] Zhou, B., Thouless, M. D., and Ward, S. M., *Int. J. Fracture* **136**, 309–326 (2005).
[55] Hill, J. C., Bennison, S. J., Klein, P. A., Foulk, J. W., Jagota, A., and Saigal, S., *Int. J. Fracture* **119**, 365–386 (2003).
[56] Hui, C. Y., Phoenix, S. L., Ibnabdeljalil, M., and Smith, R. L., *J. Mech. Phys. Solids* **43**, 1551–1585 (1995).
[57] Kramer, E. J., Microscopic and molecular fundamentals of crazing, in *Advances in Polymer Science*, H. H. Kausch (Ed.) (Springer Berlin, Heidelberg, 1983), Vol. 52/53, pp. 1–56.
[58] Kramer, E. J. and Berger, L. L., Fundamental Process of Craze Growth and Fracture, in *Advances in Polymer Science*, H. H. Kausch (Ed.) (Springer Berlin, Heidelberg, 1990), Vol. 91/92, pp. 1–67.
[59] Brown, H. R., *Macromolecules* **24**, 2752–2756 (1991).
[60] Hui, C. Y. and Kramer, E. J., *Polymer Engineering and Science* **35**, 419–425 (1995).
[61] Baljon, A. R. C. and Robbins, M. O., *Macromolecules* **34**, 4200–4209 (2001).
[62] Hui, C. Y. and Kramer, E. J., Molecular weight dependence of the fracture toughness of a craze growing into a polymer glass, in *ASME Symposium volume: Use of Plastics and Plastic Composites: Mechanics Issues*, V. K. Stokes (Ed.) (1993), pp. 309–325.
[63] Jirasek, M., *Computer methods in Applied Mechanics and Engineering* **188**, 307–330 (2000).
[64] Chaudhury, M. K. and Whitesides, G. M., *Langmuir* **7**, 1013–1025 (1991).
[65] Tang, T., Hui, C. Y., Jagota, A., and Chaudhury, M. K., *J. Adhesion* **82**, 671–696 (2006).

[66] Lake, G. J. and Thomas, A. G., *Proc. R. Soc. London, A.* **300**, 108–119 (1967).
[67] Lauterwasser, B. D. and Kramer, E. J., *Phil. Mag.* **A39**, 469–495 (1979).
[68] Elices, M., Guinea, G. V., Gomez, J., and Planas, J., *Engineering Fracture Mechanics* **69**, 137–163 (2002).
[69] Fager, L. O., Bassani, J. L., Hui, C. Y., and Xu, D. B., *Intl. J. Fracture* **52**, 119–144 (1991).
[70] Evans, A. G., Ruhle, M., Dalgleish, B. J., and Charalambides, P. G., *Material Science and Engineering* **A126**, 53–64 (1990).
[71] Liechti, K. M. and Chai, Y. S., *J. Applied Mechanics* **58**, 680–687 (1991).
[72] Zehnder, A. T. and Hui, C. Y., *Scripta Mater.* **42**, 1001–1005 (2000).
[73] Yang, Q. D. and Thouless, M. D., *Int. J. Fracture* **110**, 175–187 (2001).
[74] Park, K., Paulino, G. H., and Roesler, J. R., *J. Mech. Phys. Solids* **57**, 891–908 (2009).
[75] Rice, J. R., *J. of Applied Mechanics* **55**, 98–103 (1988).
[76] Fey and Hui, C. Y., A cohesive zone model for a crack lying along a bimaterial Interface, in *Damage Mechanics in Composites*, D. H. Allen and J. W. Ju (Eds.) (ASME Int. Mechanical Engineering Congress and Exposition, ASME Winter Annual Meeting, Nov. 6–11, 1994), pp. 37–55.
[77] ABAQUS® 6.9, Simulia, Dassault Systemes, Rising Sun Mills, Providence, RI, <http://www.simulia.com/products/abaqus_fea.html> (accessed December 2010)
[78] Camanho, P. P., Davila, C. G., and de Moura, M. F., *Journal of Composite Materials* **37**, 1415–1438 (2003).
[79] Turon, A., Camanho, P. P., Costa, J., and Davila, C. G., *Mechanics of Materials* **38**, 1072–1089 (2006).
[80] Gao, Y. F. and Bower, A. F., *Modelling and Simulation in Materials Science and Engineering* **12**, 453–463 (2004).

APPENDIX

We show that the normality rule can be used to generate traction that satisfies Eq. (48). Note that $\dot{\delta}_i = \dot{\lambda}\partial F/\partial T_i$ implies that

$$\theta = \tan^{-1}\left(\frac{\dot{\delta}_2}{\dot{\delta}_1}\right) = \tan^{-1}\left[\frac{p_2(\phi, T_1, T_2)}{p_1(\phi, T_1, T_2)}\right], \tag{A1}$$

where $p_i \equiv \partial F/\partial T_i$. However, the p_i's are not independent, since they are constrained by the equation

$$\partial p_1/\partial T_2 - \partial p_2/\partial T_1 = 0. \tag{A2}$$

In general, Eq. (A2) allows one to solve T_1 in terms of T_2 and ϕ, *i.e.*, $T_1 = q(T_2,\ \phi)$ for some function q. Substituting this into Eq. (A1) results in a nonlinear equation of the form:

$$\theta = N(\phi, T_1). \tag{A3}$$

Assuming that this equation is invertible, we have$T_1 = f_1(\phi,\ \theta)$, which is essentially Eq. (48). In exactly the same way one can show$T_2 = f_2(\phi,\ \theta)$.